Electronic Supplementary Material (ESI) for Chemical Science.

Supporting Information

Halogenation of a twisted non-polar π-system as a tool to modulate phosphorescence at room temperature

Giliandro Farias,[1] Cristian A. M. Salla,[2] Murat Aydemir,[3,4] Ludmilla Sturm,[5] Pierre Dechambenoit,[5] Fabien Durola,[5] Bernardo de Souza,[1]* Harald Bock,[5]* Andrew P. Monkman,[3]* Ivan H. Bechtold[2]*

*Corresponding authors: bernadsz@gmail.com; harald.bock@crpp.cnrs.fr; ap.monkman@durham.ac.uk; ivan.bechtold@ufsc.br;

[1]Department of Chemistry, Universidade Federal de Santa Catarina, 88040-900 Florianópolis, SC, Brazil

[2]Department of Physics, Universidade Federal de Santa Catarina, 88040-900 Florianópolis, SC, Brazil

[3]Department of Physics, Durham University, South Road, Durham, DH1 3LE, U.K.

[4]Erzurum Technical University, Department of Fundamental Sciences, Erzurum, Turkey

[5]Centre de Recherche Paul Pascal, CNRS & Université de Bordeaux, 115, av. Schweitzer, 33600 Pessac, France

Table Of Contents

Results and Discussion

Single Crystal X-ray Diffraction

Table S1. Crystallographic data.

Compound	HTX-Br	HTX-Cl
Formula	$C_{30}H_{21}Br_3$	$C_{30}H_{21}Cl_3$
FW (g·mol^{-1})	621.20	487.82
Crystal color	colourless	Colourless
Crystal size (mm)	0.45 × 0.12 × 0.05	0.28 × 0.12 × 0.05
Crystal system	trigonal	Trigonal
Space group	R-3	R-3
Temperature	120 K	120 K
***a* (Å)**	21.4648(16)	21.1589(10)
***c* (Å)**	8.7366(7)	8.6542(5)
***V* (Å^3)**	3486.0(6)	3355.4(4)
Z	6	6
d_{calc}	1.775	1.448
μ (mm^{-1})	5.225	0.428
$\theta_{min} - \theta_{max}$	1.897° - 30.071°	1.925° - 29.152°
Refl. Coll. / unique	63685 / 22266	47834 / 2016
Completeness to 2θ	0.998	1.000
R_{int}	0.0243	0.0207
Refined param./restr.	100 / 0	100 / 0
[a]R_1 ($I > 2\sigma(I)$)	0.0201	0.0284
[b]wR_2 (all data)	0.0475	0.0777
Goodness of fit	1.073	1.090

[a] $R_1 = \Sigma||F_0| - |F_C||/\Sigma|F_0|$ and [b] $wR_2 = [\Sigma w(F_0^2 - F_C^2)^2/\Sigma w(F_o^2)^2]^{1/2}$

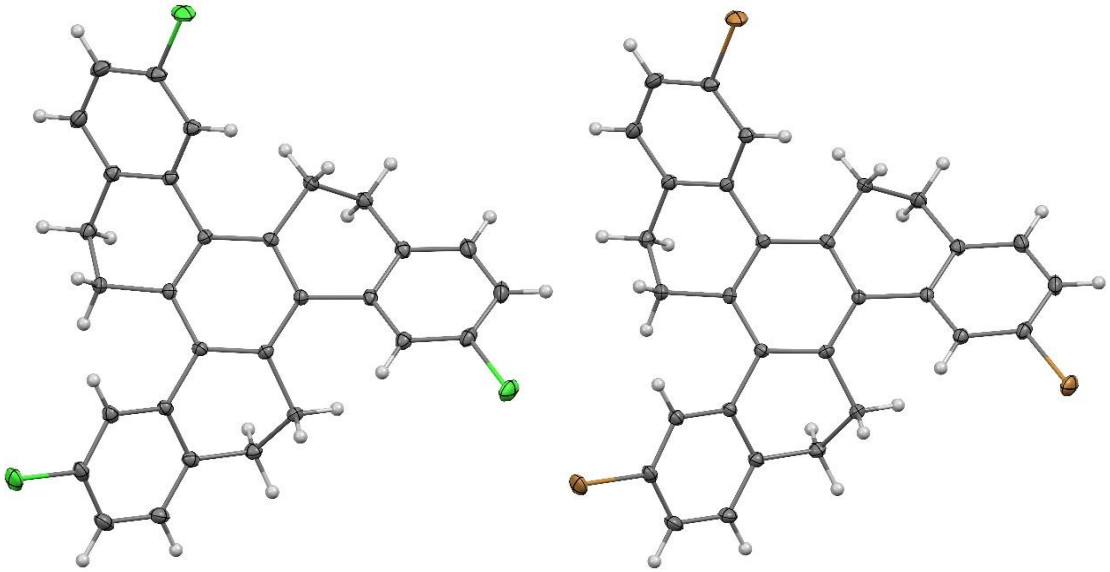

Figure S1. ORTEP plot of the molecular structure. ORTEP-type views (left and right) of **HTX-Cl** (left) and **HTX-Br** (right) along the *(ab)* plane at 120 K; C grey, Br orange, Cl green, H white. Thermal ellipsoids of the non-hydrogen atoms are depicted at a 50 % probability level.

Room-temperature UV-Vis Investigations

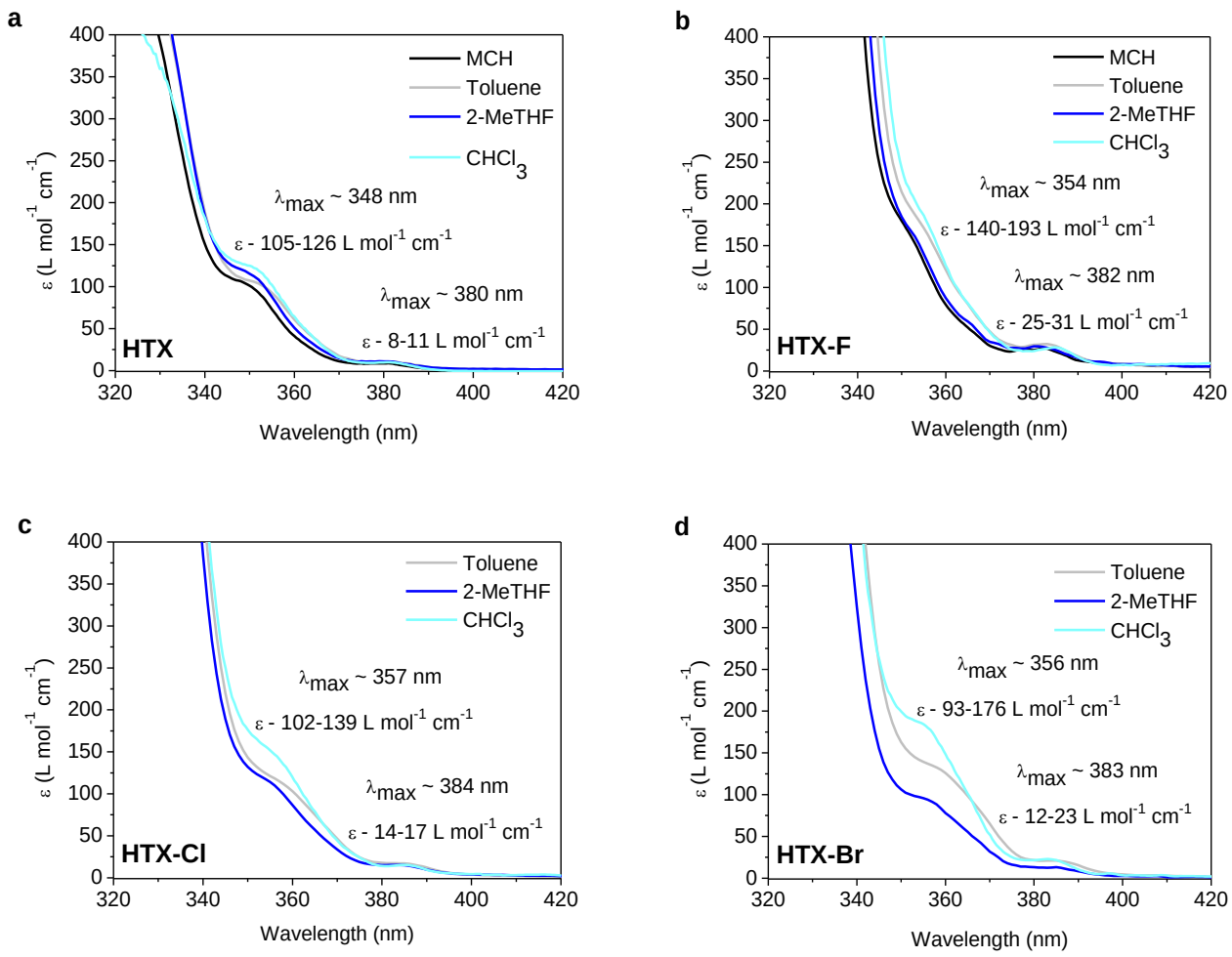

Figure S2. Absorption in different solvents. Optical absorption spectra in methylcyclohexane, toluene, 2-MeTHF and chloroform solutions (10^{-3} mol L^{-1}). **HTX-Cl** and **HTX-Br** were not soluble in methylcyclohexane.

Table S2. Comparison between experimental and calculated OS within PBE0/def2-TZVP(-f) in 2-MeTHF.

State		∫εdυ	*f* [a]	*f*
S_1	**HTX**	7920	0.00003	0.00017
	HTX-F	28895	0.00012	0.00166
	HTX-Cl	22395	0.00009	0.00037
	HTX-Br	12459	0.00005	0.00017
S_2	**HTX**	129641	0.00056	0.00070
	HTX-F	340467	0.00147	0.12670
	HTX-Cl	188206	0.00081	0.00279
	HTX-Br	174209	0.00075	0.00931

[a] $f = 4.32\times10^{-9}\int\varepsilon d\upsilon$, where υ is the wavenumber in cm^{-1}.

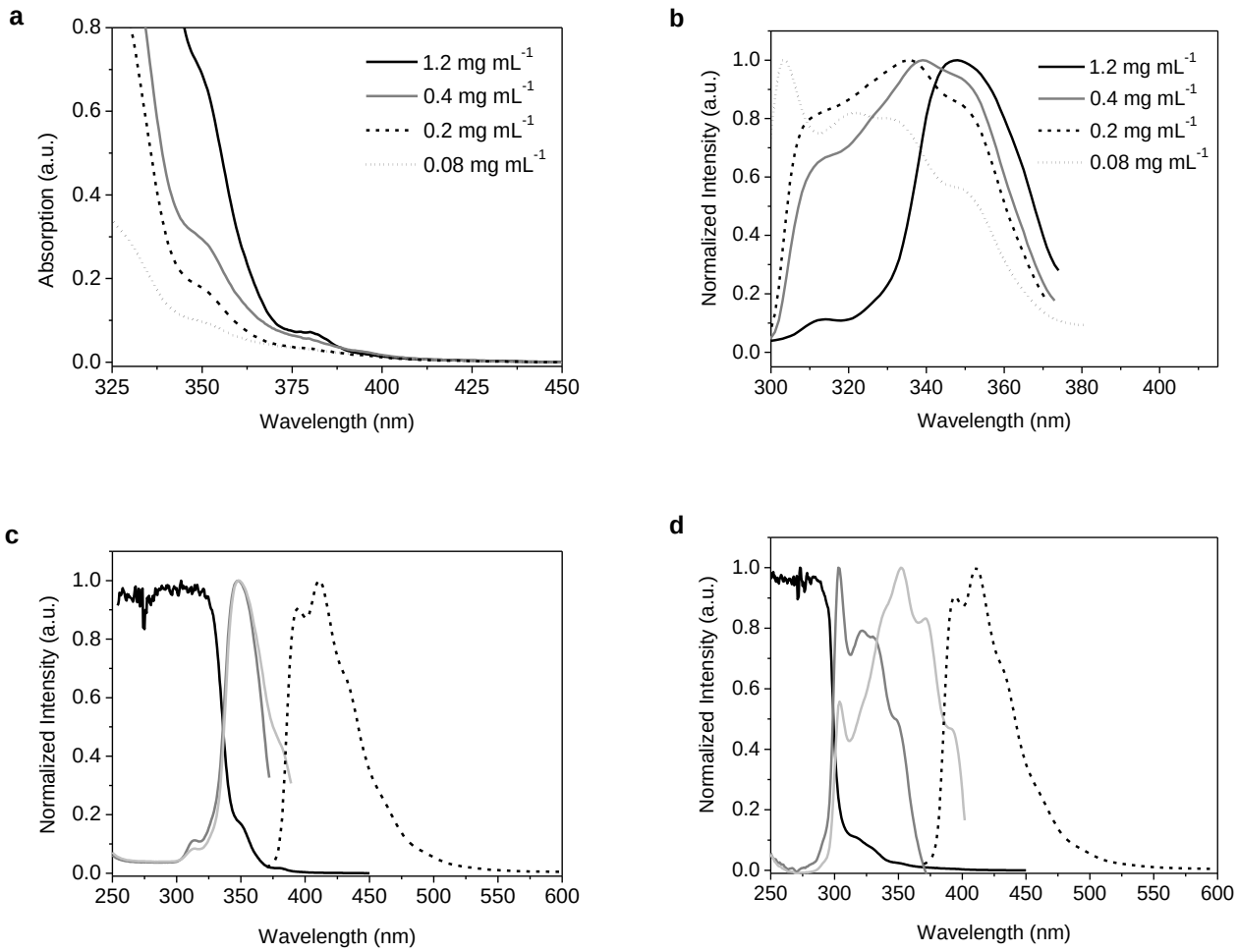

Figure S3. Effect of concentration on absorption and emission. (**a**) Absorption and (**b**) excitation spectra at 390 nm of **HTX** in 2-MeTHF solution with different concentrations. The excitation spectra change with concentration because of the inner filter effect. At high concentration, the excitation light excites only a thin layer at the front face of the cuvette and using 90º angle collection, emission mainly from the center of the cuvette is collected. Thus, the excitation spectra at high concentration becomes distorted at high energy. However, on the absorption band edge, they all become very similar. Absorption (black line), excitation monitored at 390 nm (grey line), excitation monitored at 410 nm (light grey line) and emission spectra (dashed black line) in 2-MeTHF solution (**c**) 1.2 mg mL^{-1} and (**d**) 0.08 mg mL^{-1}.

Steady-state Emission and Quantum Yield in Solution

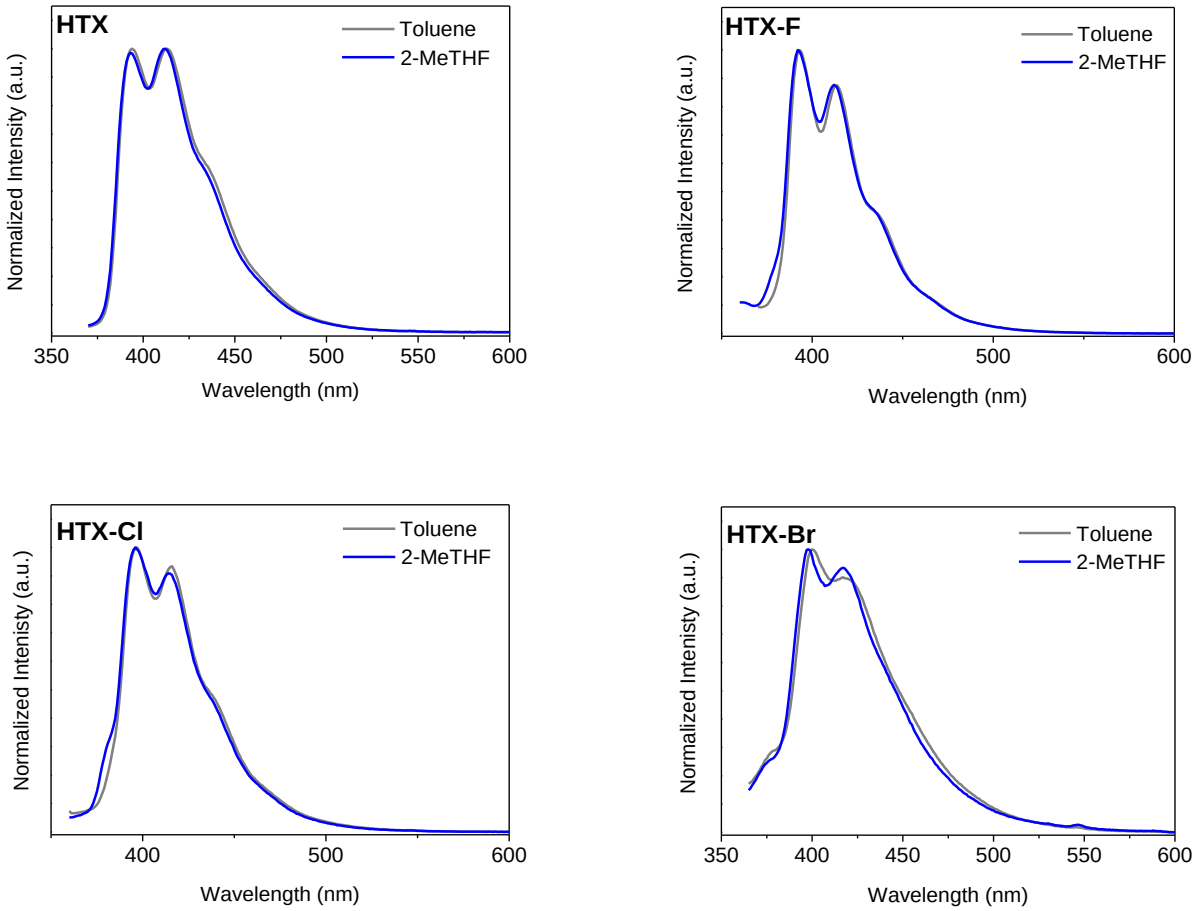

Figure S4. Emission spectra in dilute toluene and 2-MeTHF solutions.

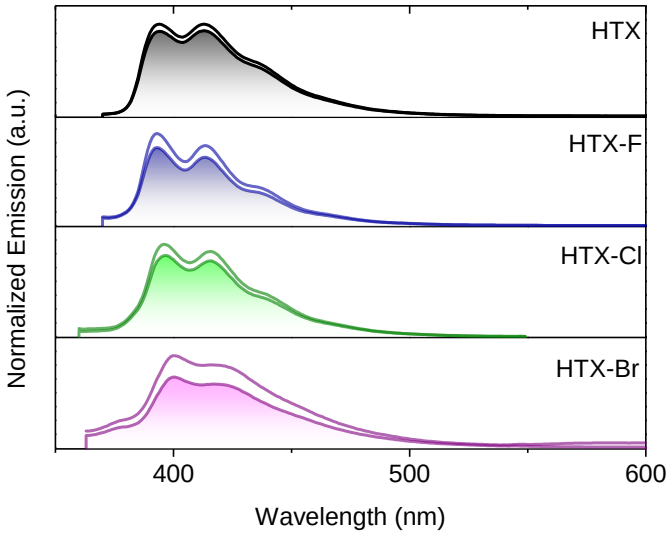

Figure S5. Emission spectra in degassed and aerated diluted toluene solution. The solid lines are the steady-state spectra at RT collected in degassed solution and the filled areas collected in aerated solution.

Table S3. RT fluorescence quantum yields in different solvents. The error of Φ was ±0.004.

	HTX	**HTX-F**	**HTX-Cl**	**HTX-Br**
Φ_{PF} in 2-MeTHF	0.211	0.328	0.078	0.011
Φ_{DF} in 2-MeTHF	0.185	0.102	0.021	0.002
Φ_{PF} in toluene	0.179	0.128	0.050	0.012
Φ_{DF} in toluene	0.015	0.021	0.006	0.004

Time-correlated Single-photon Counting Emission Decay in Solution

357nm Excitation Source

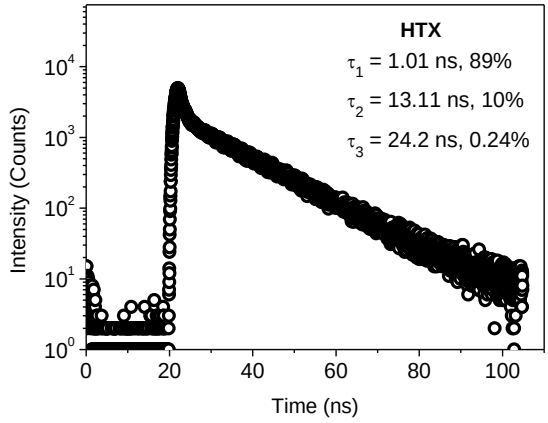

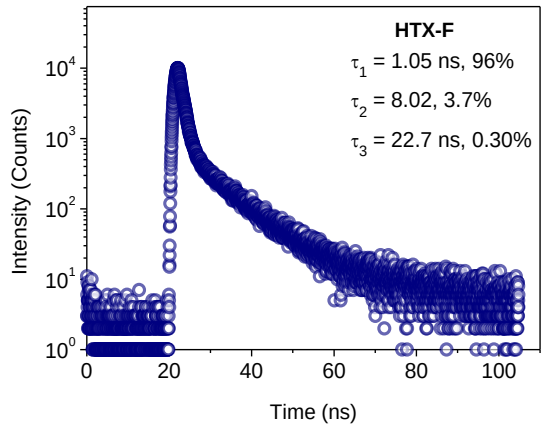

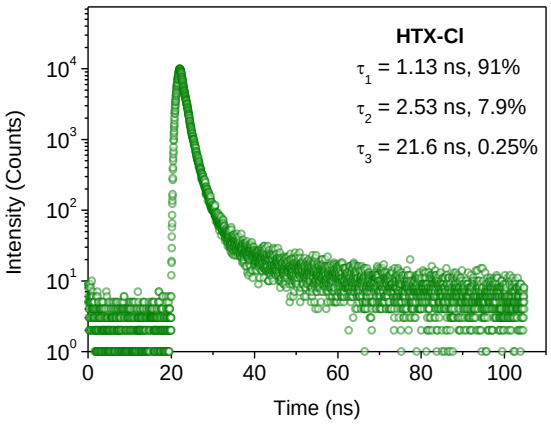

405 nm Excitation Source

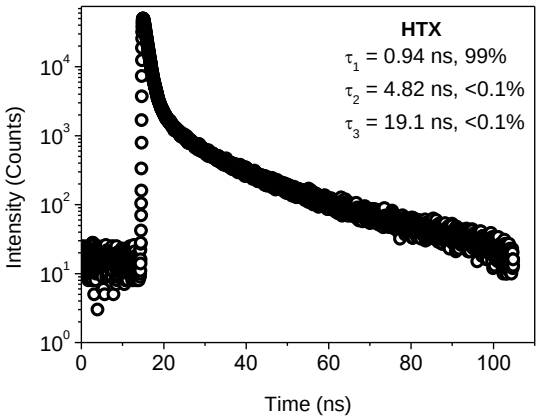

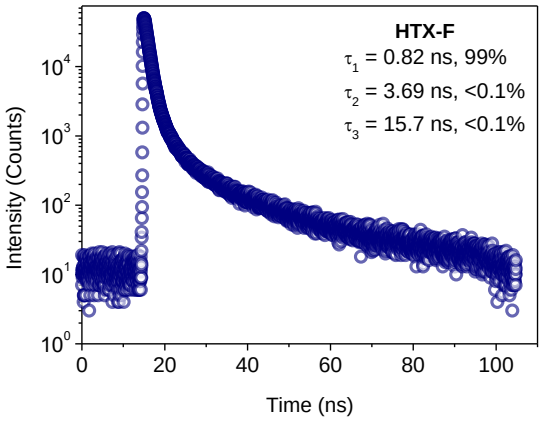

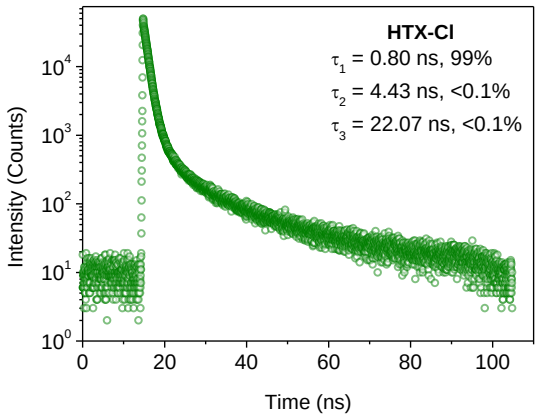

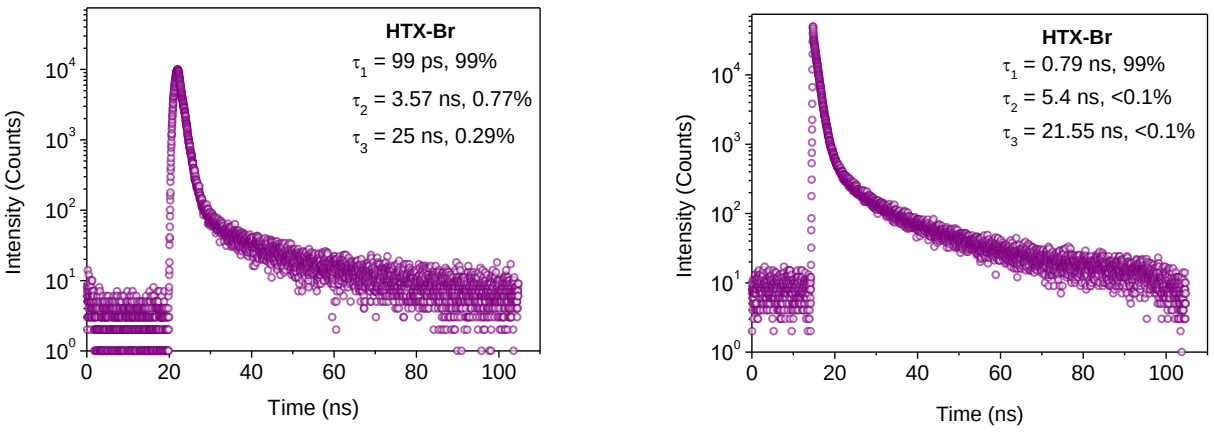

Figure S6. Time-correlated single-photon counting emission decay curves in diluted 2-MeTHF solution at 420 nm. Left column: Excited at 357nm; Right column: Excited at 405nm.

Table S4. Emission lifetimes and their relative amplitudes from TCSPC measurements in 2-MeTHF solutions.

	HTX	**HTX-F**	**HTX-Cl**	**HTX-Br**
τ_1 (A_1) [a] (ns)	1.01 (0.89)	1.05 (0.96)	1.13 (0.91)	0.99 (0.99)
τ_2 (A_2) [a] (ns)	13.11 (0.10)	8.02 (0.036)	2.53 (0.079)	3.57 (7.7×10^{-3})
τ_3 (A_3) [a] (ns)	24.20 (2.4×10^{-3})	22.7 (2.5×10^{-3})	21.6 (2×10^{-3})	25.00 (2.9×10^{-3})
τ_1 (A_1) [b] (ns)	0.94 (0.99)	0.82 (0.99)	0.80 (0.99)	0.79 (0.99)
τ_2 (A_2) [b] (ns)	4.82 (7.4×10^{-6})	3.69 (3.06×10^{-8})	4.43 (6.4×10^{-9})	5.5 (2.1×10^{-9})
τ_3 (A_3) [b] (ns)	19.1 (5.2×10^{-7})	15.7 (1.51×10^{-10})	22.07 (4.12×10^{-11})	21.55 (4.4×10^{-11})

[a] 357nm excitation source is used (<1.4 ns pulse duration); [b] 405 nm excitation right on the edge. Excitation into the very weak 370-400 absorption band (405 nm excitation) yields mono-exponential decays close to the IRF.

Time-Resolved and Power Dependence Measurements in Solution

The time-resolved PF decay of **HTX** was best fitted with a monoexponential decay of τ = 12.7 ns at RT and only a slight change in the PF decay is observed on cooling down to 90 K (Figure S7 a). The long-lived component was best fitted with a triexponential decay of τ = 8.3 μs (A_1 = 30%), τ = 89.6 μs (A_2 = 57%) and, τ = 293.7 μs (A_3 = 13%) at RT. On cooling down to 90 K the long-lived component was best fitted with a monoexponential decay of τ = 498 ms. Normalized spectra taken over the entire measurement (Figure S7 b**)** show that from TD = 1.1

ns to around TD = 100 ns (black line), an emission peak centered at 421 nm is observed having a weak vibronic structure. Around TD = 1.6 µs (grey line) an emission centered at 424 nm is observed, which is ascribed to the delayed emission from TTA. Then, after TD = 27 µs, a continuous red-shift is observed and the band becomes clearly gaussian shaped, which is associated with the mixing of emitting states and growing dominance of the faster Ph emission (light grey line, TD = 422 µs – 1.2 ms). Normalized spectra at 90 K (Figure S7 c**)** show that the emission at TD = 1.1 ns is centered at 412 nm. No obvious relaxation of this state is seen over 170 ns. From TD = 376 µs until TD = 8.4 ms the slower Ph emission is observed at this temperature. Figure S7 d shows the peak position in function of TD for RT and 90 K.

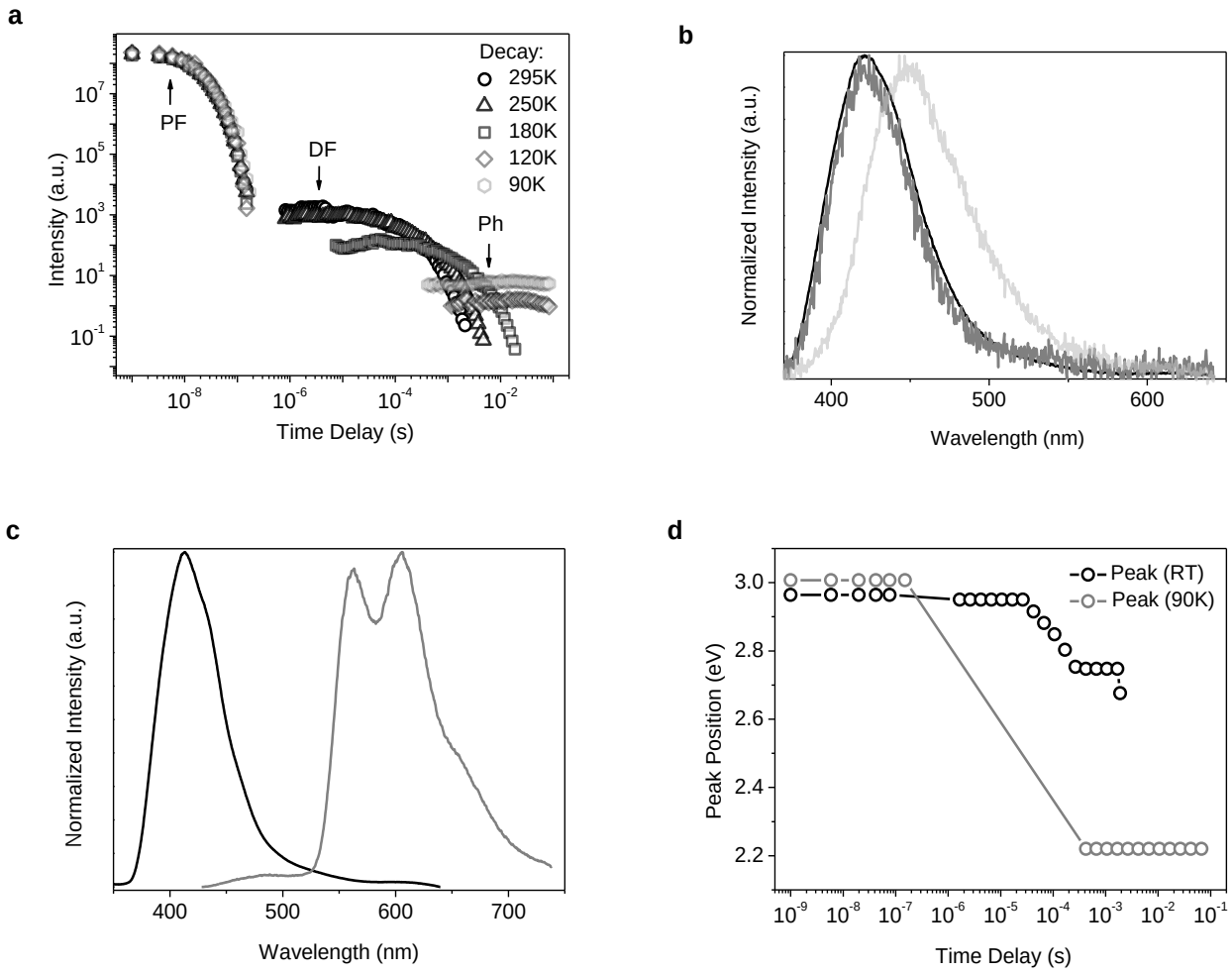

Figure S7. Time-resolved measurements for **HTX**. (**a**) Time-resolved decay of **HTX** in 2-MeTHF as function of temperature. (**b**) Normalized spectra taken after different TD at RT for **HTX**. TD = 1.1 – 100 ns (black line); TD = 1.6 – 27 µs (grey line); TD = 422 µs – 1.2 ms (light grey line). (**c**) Normalized spectra taken over after different TD at 90 K for **HTX**. TD = 1.1 – 170 ns (black line); TD = 376 µs – 8.4 ms (grey line). (**d**) Shift of the emission maximum from **HTX** at RT and 90 K.

The excitation wavelength was 355 nm. All measurements were performed in the absence of oxygen.

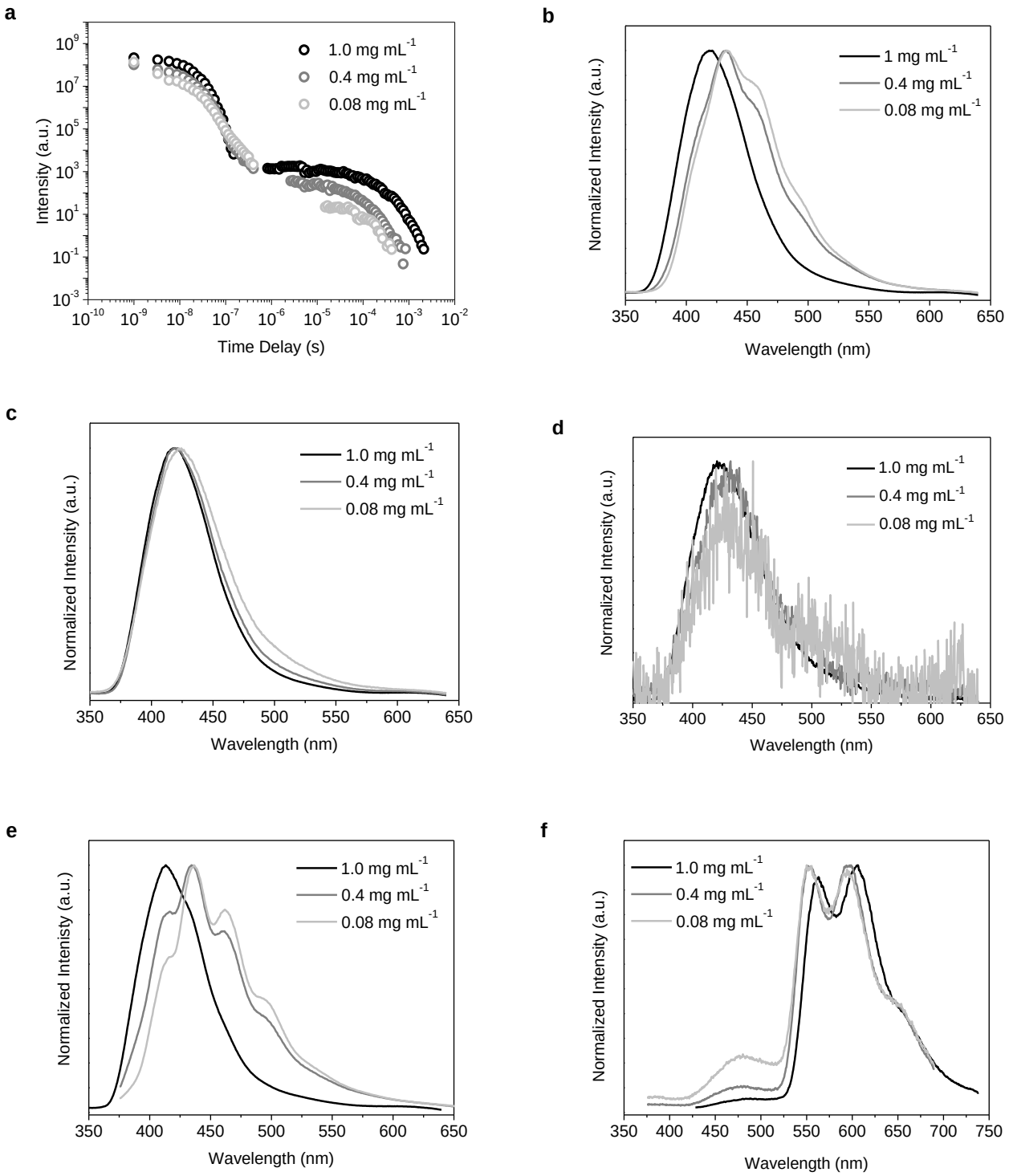

Figure S8. Time-resolved measurements for **HTX** with different concentrations. (**a**) Time-resolved decay of **HTX** in 2-MeTHF solution with different concentrations. For the 0.08 mg L^{-1} solution the PF decay turns into a triexponential decay of τ = 1.2 ns (A_1 = 4%), τ = 13.24 ns (A_2 = 95%) and, τ = 74.79 (A_3 = 1%) at RT. (**b**) Normalized spectra taken with TD = 1.1 ns for **HTX**

in 2-MeTHF solution with different concentrations at RT. (**c**) Normalized spectra taken with TD = 5.85 ns for **HTX** in 2-MeTHF solution with different concentrations at RT. (**d**) Normalized spectra taken during the long-lived component for **HTX** in 2-MeTHF solution with different concentrations at RT. **(e)** Normalized spectra taken with TD = 1.1 ns for **HTX** in 2-MeTHF solution with different concentrations at 80 K. (**f**) Ph normalized spectra of **HTX** in 2-MeTHF solution with different concentrations at 90 K. The excitation wavelength was 355 nm. All measurements were performed in the absence of oxygen.

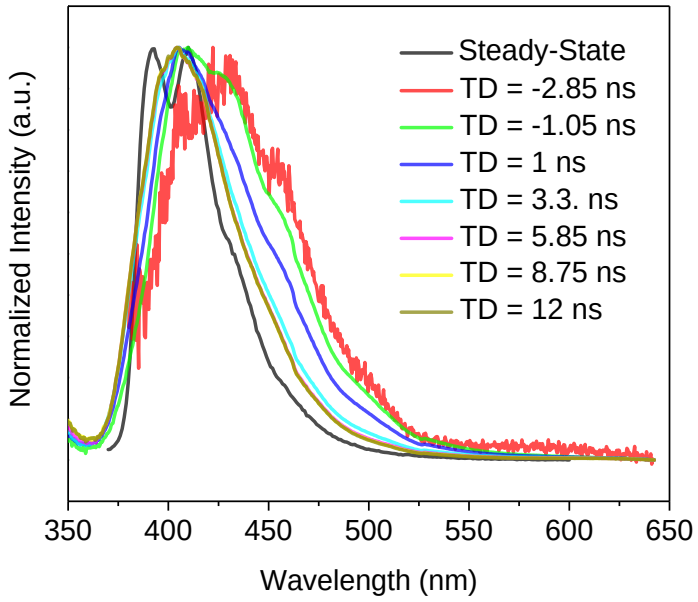

Figure S9. Normalized emission spectra taken with different TD for **HTX** in 2-MeTHF solution at RT.

For **HTX-F** the PF decay was best fitted with a biexponential decay of τ = 9.4 ns (A_1 = 99%) and τ = 48.9 ns (A_2 = 1%) at RT and only a slight change in the PF decay is observed on cooling down to 90 K (Figure S10 a). The long-lived component was best fitted with a triexponential decay of τ = 7.8 µs (A_1 = 58%), τ = 128 µs (A_2 = 34%) and, τ = 471 µs (A_3 = 8%) at RT. On cooling down to 90 K the long-lived component was best fitted with a monoexponential decay of τ = 766 ms. No long-lived signal was observed at 120 K. Normalized spectra taken over the entire measurement (Figure S10 b**)** shows that from TD = 1.1 ns to around TD = 88 ns (black line), an emission peak centered at 419 nm is observed having weak vibronic structure. Then a blue shift is observed leading to a new emission peak centered at 411 nm from TD = 101 to 116 ns (grey line). Around TD = 2.65 µs (light grey line) an emission centered at 419 nm is observed again, which is ascribed to the delayed emission from TTA. Then, after TD = 67 µs,

a continuous red-shift is observed and the band becomes clearly gaussian shaped, which is associated with the mixing of emitting states and growing dominance of the faster Ph decay (royal line, TD = 75 µs – 2.12 ms). At 90 K (Figure S10 c**)** the emission from TD = 1.1 to 101 ns is centered at 415 nm (black line) and from TD = 115 to 150 ns at 408 nm (grey line). From TD = 422 µs until TD = 8.4 ms (light grey line) the slower Ph emission is observed. Figure S10 d shows the peak position in function of TD for RT and 90 K.

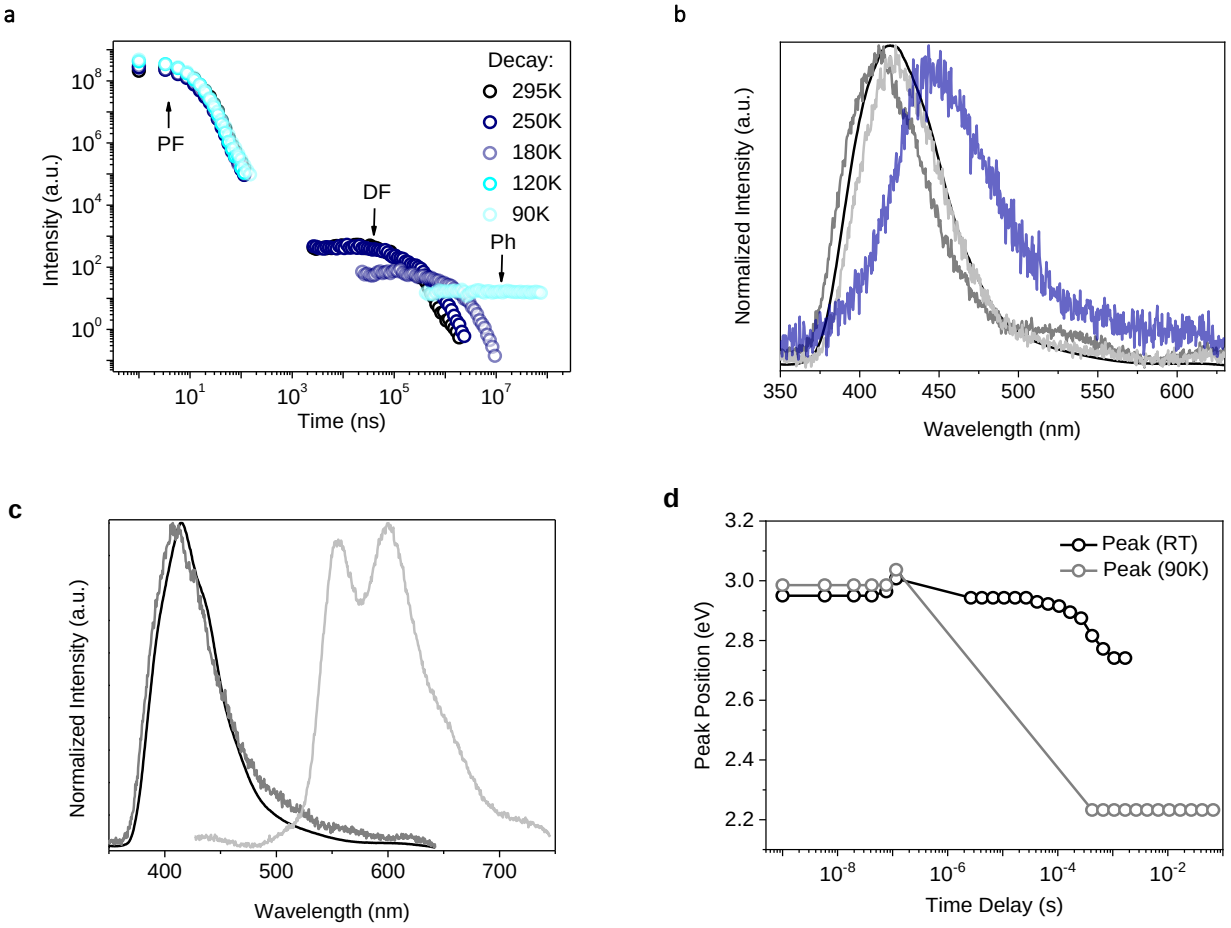

Figure S10. Time-resolved measurements for **HTX-F**. (**a**) Time-resolved decay of **HTX-F** in 2-MeTHF as function of temperature. (**b**) Normalized spectra taken after different TD at RT for **HTX-F**. TD = 1.1 – 88 ns (black line); TD = 101 – 116 ns (grey line); TD = 2.65 – 67 µs (light grey line); TD = 75 µs – 2.12 ms (royal line). (**c**) Normalized spectra taken after different TD at 90 K for **HTX-F**. TD = 1.1 – 101 ns (black line); TD = 115 – 150 ns (grey line); TD = 422 µs – 8.4 ms (light grey line). (**d**) Shift of the emission maximum from **HTX-F** at RT and 90 K. The excitation wavelength was 355 nm. All measurements were performed in the absence of oxygen.

For **HTX-Cl** the PF decay was best fitted with a biexponential decay of τ = 2.46 ns (A_1 = 98%) and τ = 31.5 ns (A_2 = 2%) at RT (Figure S11 a). The long-lived component was best fitted with a triexponential decay of τ = 3.6 µs (A_1 = 30%), τ = 109 µs (A_2 = 66%) and, τ = 344 µs (A_3 = 4%) at RT. For this compound on cooling down a new exponential is observed in the ns time frame, i.e. the decay curve at 120 K was best fitted with a triexponential decay of τ = 4.5 ns (A_1 = 90.6%), τ = 29.3 ns (A_2 = 9%) and, τ = 222 ns (A_3 = 0.4%). On cooling down to 90 K the long-lived component was best fitted with a monoexponential decay of τ = 315 ms. No long-lived signal was observed at 120 K. Normalized spectra taken over the entire measurement (Figure S11 b) shows that from TD = 1.1 ns to around TD = 24 ns (black line), an emission peak centered at 424 nm is observed having weak vibronic structure. Then a blue shift is observed leading to a new emission peak centered at 412 nm from TD = 30 to 88 ns (grey line). Around TD = 2.4 µs (light grey line) an emission centered at 424 nm is observed again, which is ascribed to the delayed emission. Then, after TD = 75 µs, a continuous red shift is observed and the band becomes clearly gaussian shaped, which is associated with the mixing of emitting states and growing dominance of the faster Ph (green line, TD = 133 to 670 µs). The emission at 90 K (Figure S11 c) from TD = 1.1 to 132 ns is centered at 424 nm (black line) and from TD = 150 to 927 ns at 412 nm (grey line). From TD = 422 µs until TD = 6.7 ms (light grey line) the slower Ph emission is observed. Figure S11 d shows the peak position in function of TD for RT and 90 K.

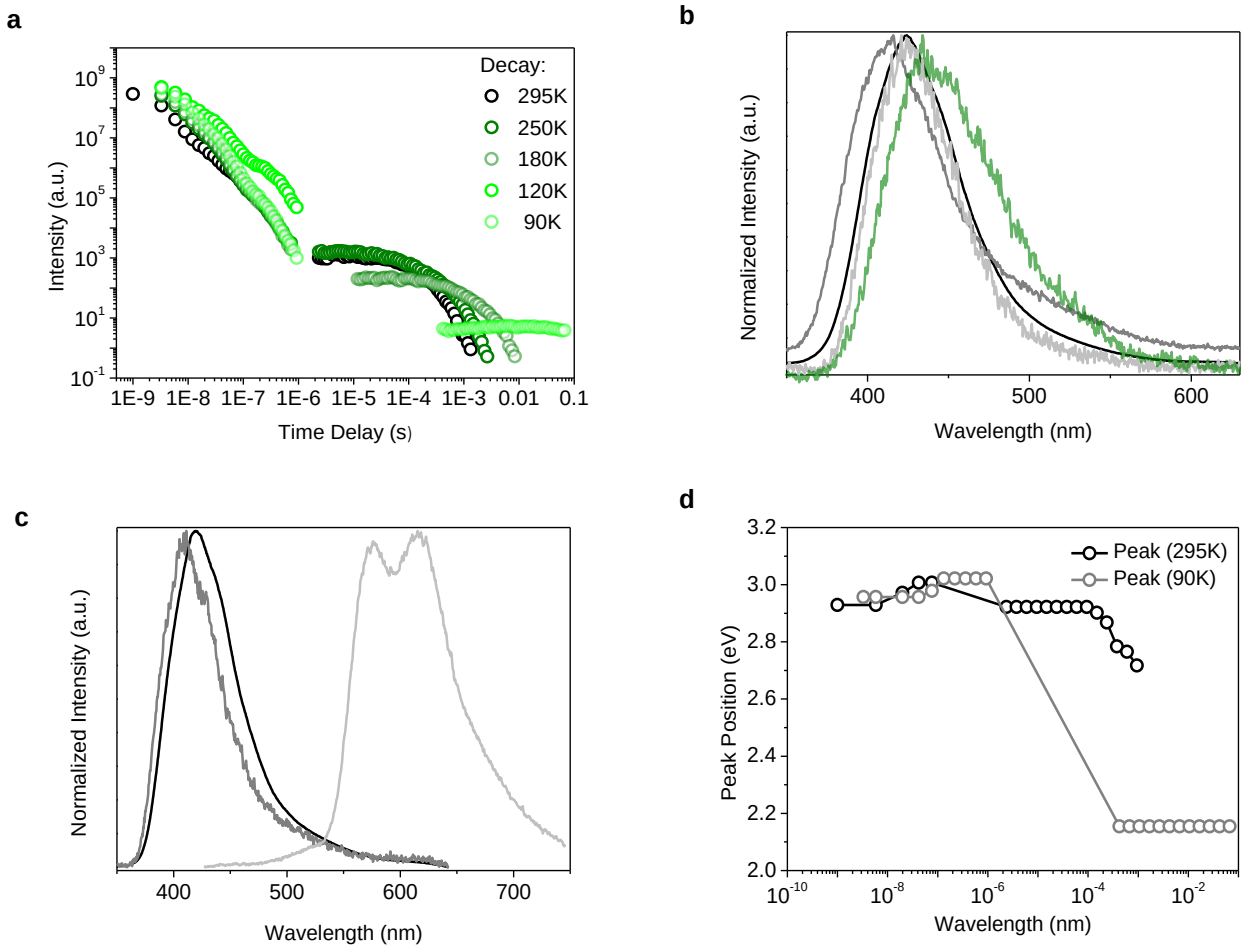

Figure S11. Time-resolved measurements for **HTX-Cl**. (**a**) Time-resolved decay of **HTX-Cl** in 2-MeTHF as function of temperature. (**b**) Normalized spectra taken after different TD at RT for **HTX-Cl**. TD = 1.1 – 24 ns (black line); TD = 30 – 88 ns (grey line); TD = 2.40 – 75 µs (light grey line); TD = 133 – 670 µs (green line). (**c**) Normalized spectra taken after different TD at 90 K for **HTX-Cl**. TD = 1.1 – 132 ns (black line); TD = 150 – 927 ns (grey line); TD = 422 µs – 6.7 ms (light grey line). (**d**) Shift of the emission maximum from **HTX-Cl** at RT and 90 K. The excitation wavelength was 355 nm. All measurements were performed in the absence of oxygen.

For **HTX-Br** the PF decay was best fitted with a biexponential decay of τ = 1.2 ns (A_1 = 72%) and τ = 7.1 ns (A_2 = 28%) at RT (Figure S12 a). The long-lived component was best fitted with a monoexponentially decay of τ = 805 µs. On cooling down to 90 K the long-lived component was best fitted with a monoexponentially decay of τ = 14.8 ms. Normalized spectra taken over the entire measurement (Figure S12 b) shows that from TD = 1.1 ns to around TD = 9 ns (black line), an emission peak centered at 420 nm is observed having weak vibronic structure. Then a blue shift is observed leading to a new emission peak centered at 415 nm from TD = 12 to 66 ns (grey line). Around TD = 12 to 669 µs (light grey line) the Ph emission

(λ_{max} = 558 nm) can be seen at RT along with the TTA emission (λ_{max} = 420 nm). Then, from TD = 751 µs to 3.7 ms (purple line) faster Ph (λ_{max} = 440 nm) is observed along with the slower Ph. At 90 K (Figure S12 c) from TD = 1.1 ns to around TD = 3.3 ns (black line), the emission peak centered at 417 nm is observed, then blue shift to 410 nm and the emission is observed until TD = 101 ns (grey line). Around TD = 12 to 30 µs (light grey line) the slower Ph emission (λ_{max} = 558 nm) can be seen at RT along with a weak TTA emission. Then, from TD = 34 µs to 7.5 ms (purple line) a growing intensity of faster Ph at 440 nm is observed along with the dominant slower Ph at 558 nm. Figure S12 d shows the peak position in function of TD for RT and 90 K.

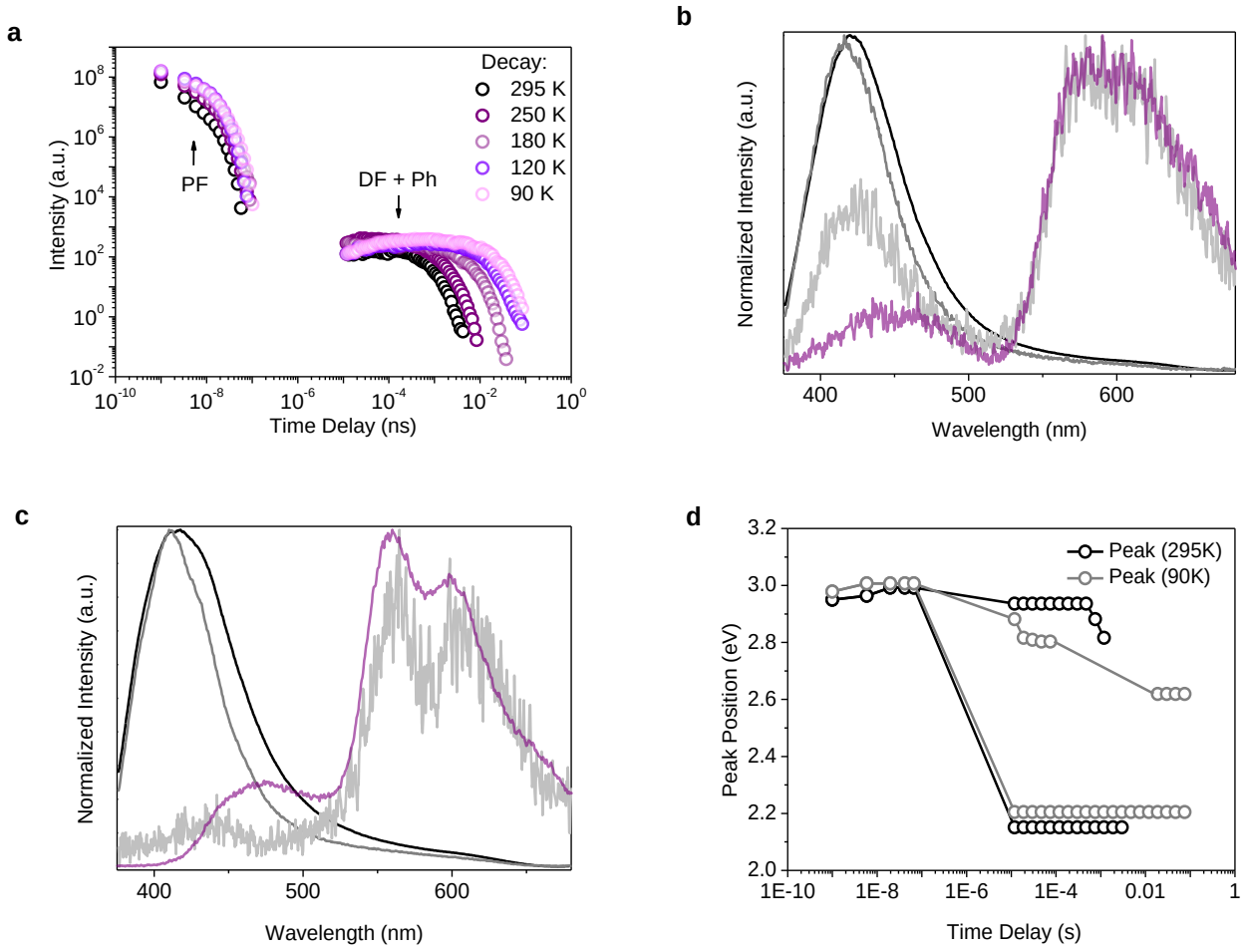

Figure S12. Time-resolved measurements for **HTX-Br**. (**a**) Time-resolved decay of **HTX-Br** in 2-MeTHF as function of temperature. (**b**) Normalized spectra taken after different TD at RT for **HTX-Br**. TD = 1.1 – 9 ns (black line); TD = 12 - 66 ns (grey line); TD = 12 – 699 µs (light grey line); TD = 751 µs - 3.7 ms (purple line). (**c**) Normalized spectra taken after different TD at 90 K for **HTX-Br**. TD = 1.1 – 3.3 ns (black line); TD = 5.85 - 101 ns (grey line); TD = 12 – 30 µs (light grey line); TD = 34 µs – 7.5 ms (purple line). (**d**) Shift of the emission maximum from **HTX-Br** at

RT and 90 K. The excitation wavelength was 355 nm. All measurements were performed in the absence of oxygen.

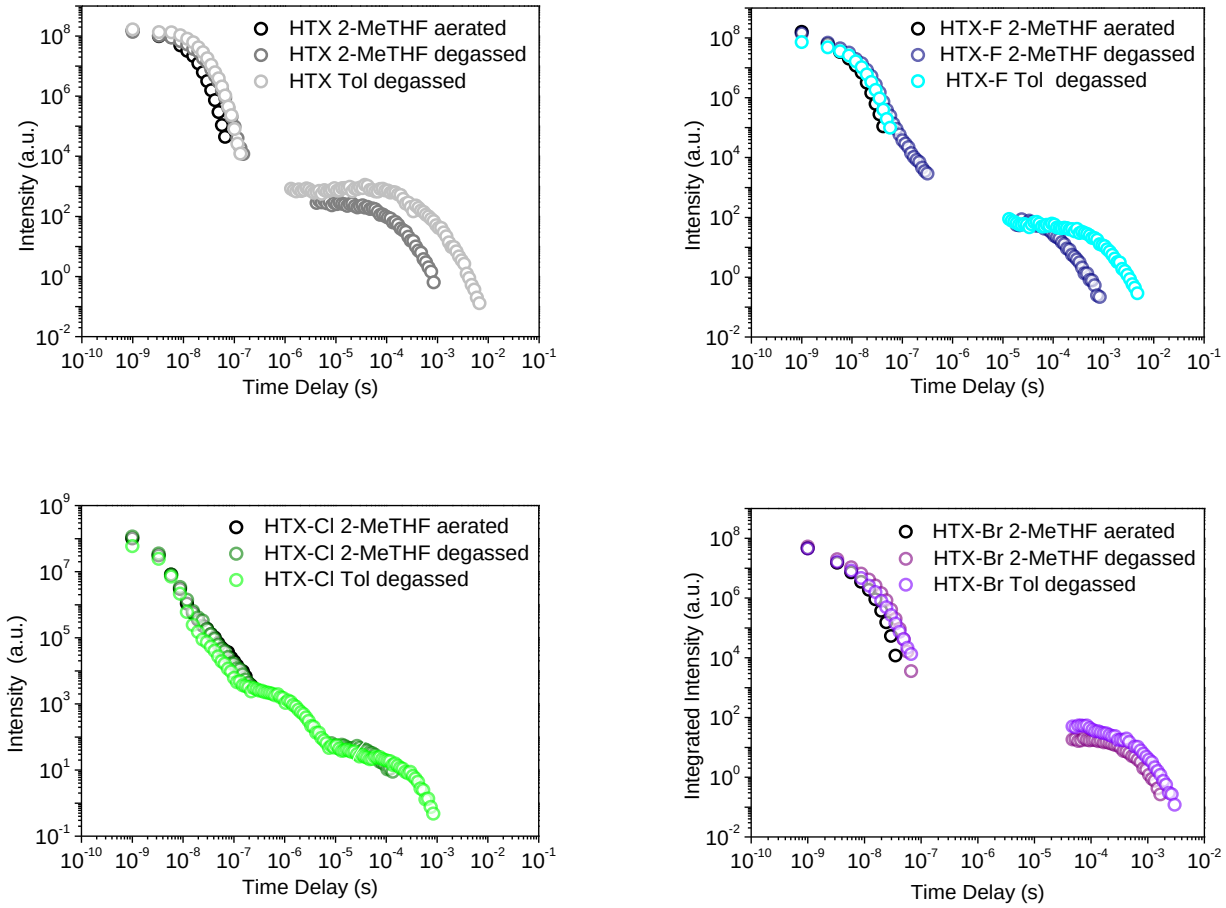

Figure S13. Time-resolved decay as function of the environment. The major difference in toluene solutions is related to the faster Ph emission with high intensity. In aerated solutions the long-lived decay is not observed due to the oxygen quenching.

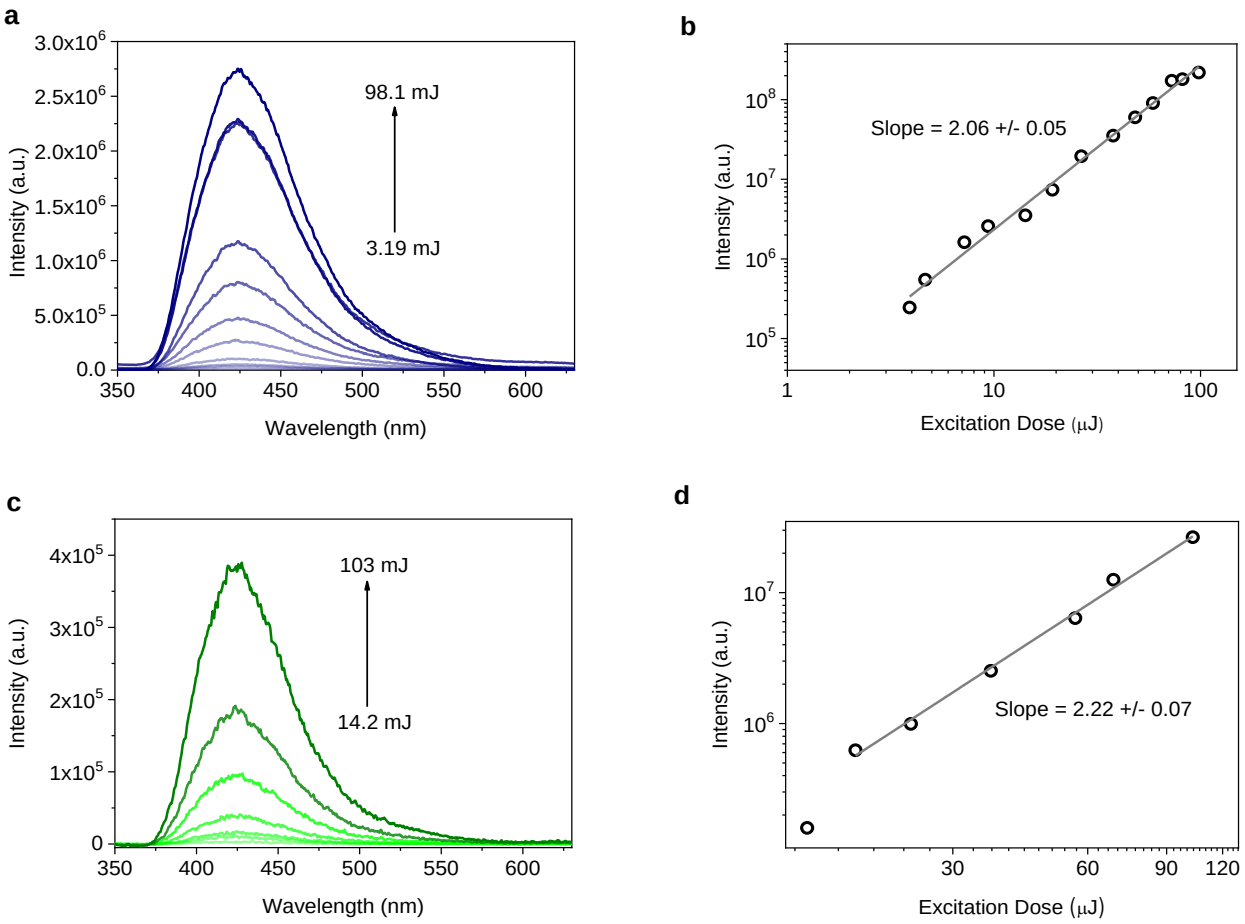

Figure S14. Emission spectra and intensity as a function of the laser excitation dose. **HTX-F** (**a** and **b**, 337 nm, TD = 20 μs, Ti = 200 μs), and **HTX-Cl** (**c** and **d**, 337 nm, TD = 5 μs, Ti = 18 μs).

Absorption, Time-resolved Emission Decay and Quantum Yield in Powder

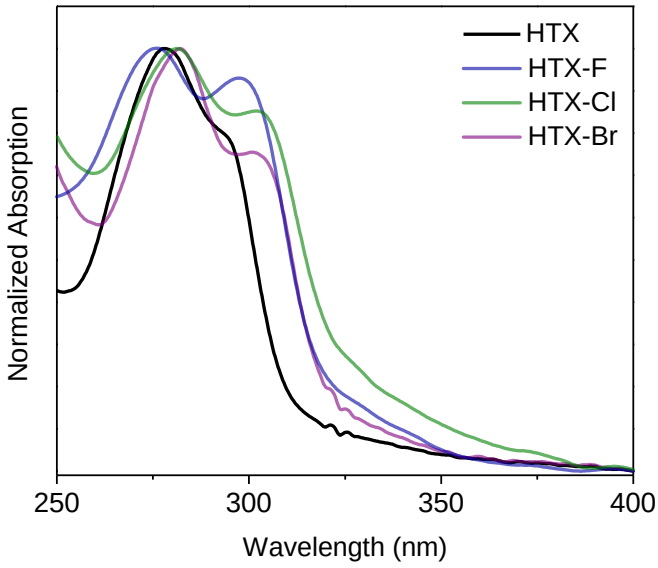

Figure S15. Normalized absorption spectra in undissolved powder at RT.

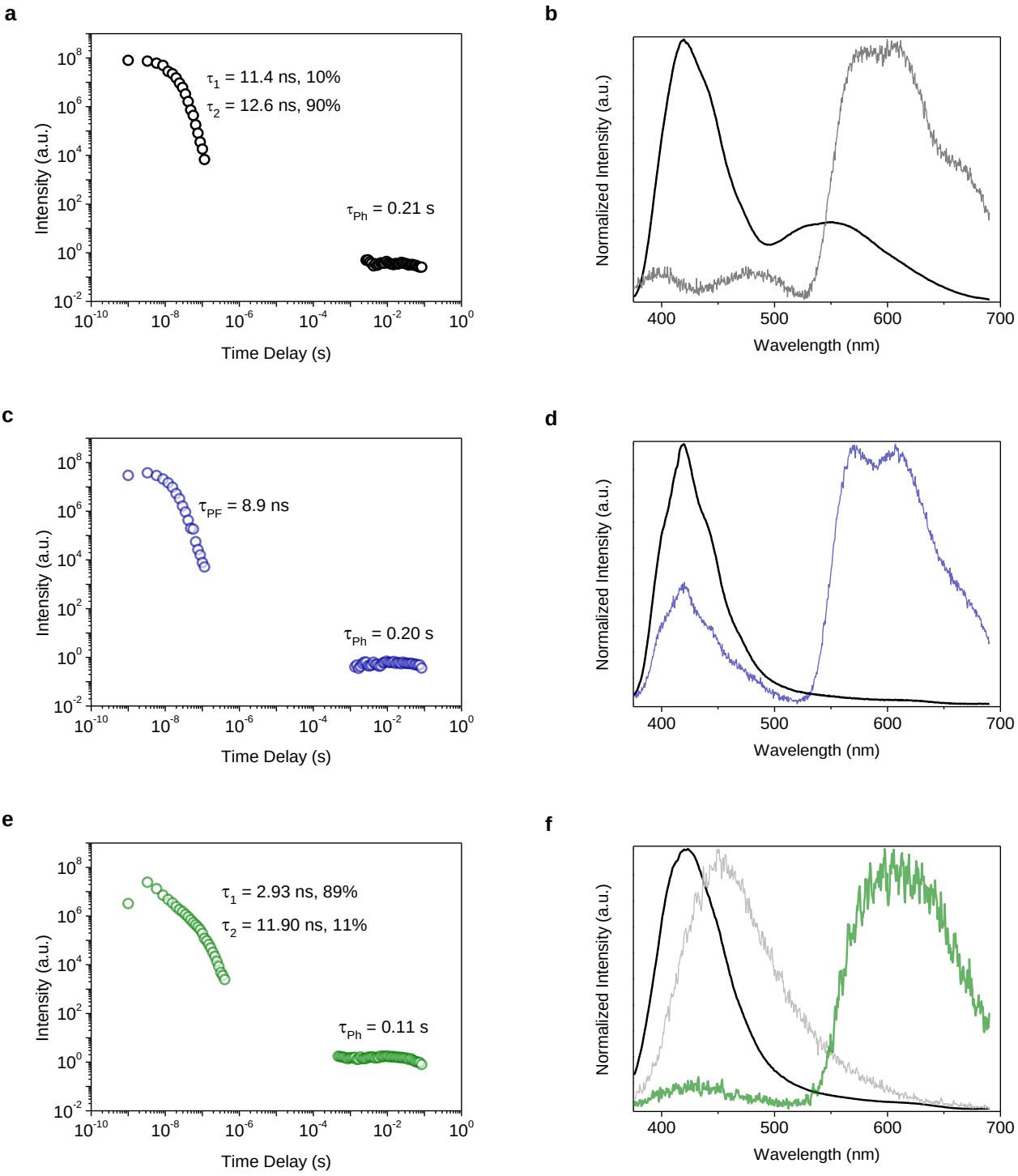
a
b
c
d
e
f
Intensity (a.u.)
Time Delay (s)
τ1 = 11.4 ns, 10%
τ2 = 12.6 ns, 90%
τPh = 0.21 s
Normalized Intensity (a.u.)
Wavelength (nm)
τPF = 8.9 ns
τPh = 0.20 s
τ1 = 2.93 ns, 89%
τ2 = 11.90 ns, 11%
τPh = 0.11 s

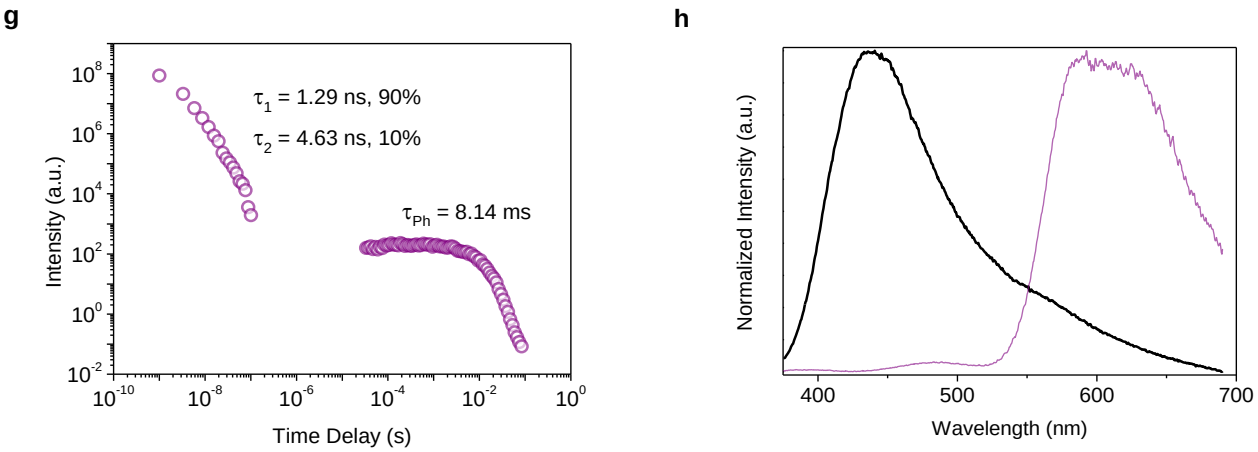

Figure S16. Time-resolved measurements in the powder at RT. **(a)** Time-resolved decay of **HTX** in powder at RT. **(b)** Normalized spectra taken after different TD at RT for **HTX**. TD = 1.1 – 116 ns (black line); TD = 2.7 – 84.3 ms (grey line). **(c)** Time-resolved decay of **HTX-F** in powder at RT. **(d)** Normalized spectra taken after different TD at RT for **HTX-F**. TD = 1.1 – 116 ns (black line); TD = 1.3 – 84.3 ms (royal line). **(e)** Time-resolved decay of **HTX-Cl** in powder at RT. **(f)** Normalized spectra taken after different TD at RT for **HTX-Cl**. TD = 1.1 ns (black line); TD = 24 - 404 ns (light grey line); TD = 473 µs – 84.3 ms (olive line). **(g)** Time-resolved decay of **HTX-Br** in powder at RT. **(h)** Normalized spectra taken after different TD at RT for **HTX-Br**. TD = 1.1 – 101 ns (black line); TD = 335 µs – 84.3 ms (purple line).

Table S5. Emission quantum yield in powder in powder at RT. The error in Φ was ±0.002.

	HTX	**HTX-F**	**HTX-Cl**	**HTX-Br**
Φ_{PF}	0.410	0.197	0.103	0.012
Φ_{Ph}	0.062	0.033	0.027	0.063

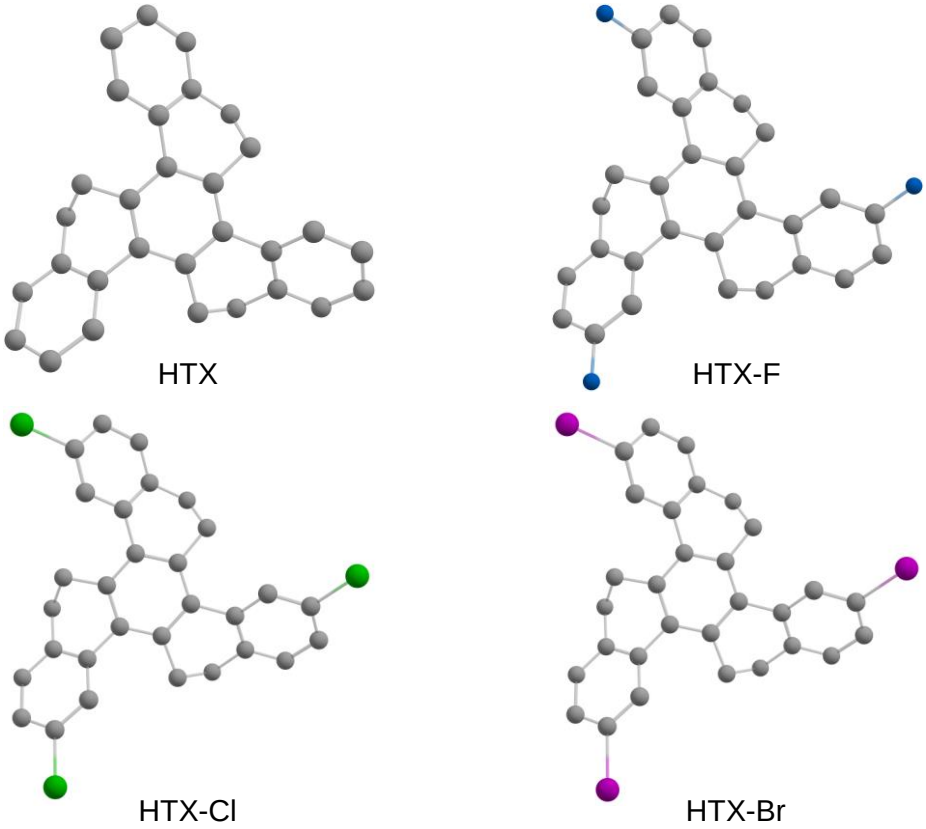

Figure S17. Optimized ground state geometries using PBE0/def2-TZVP(-f).

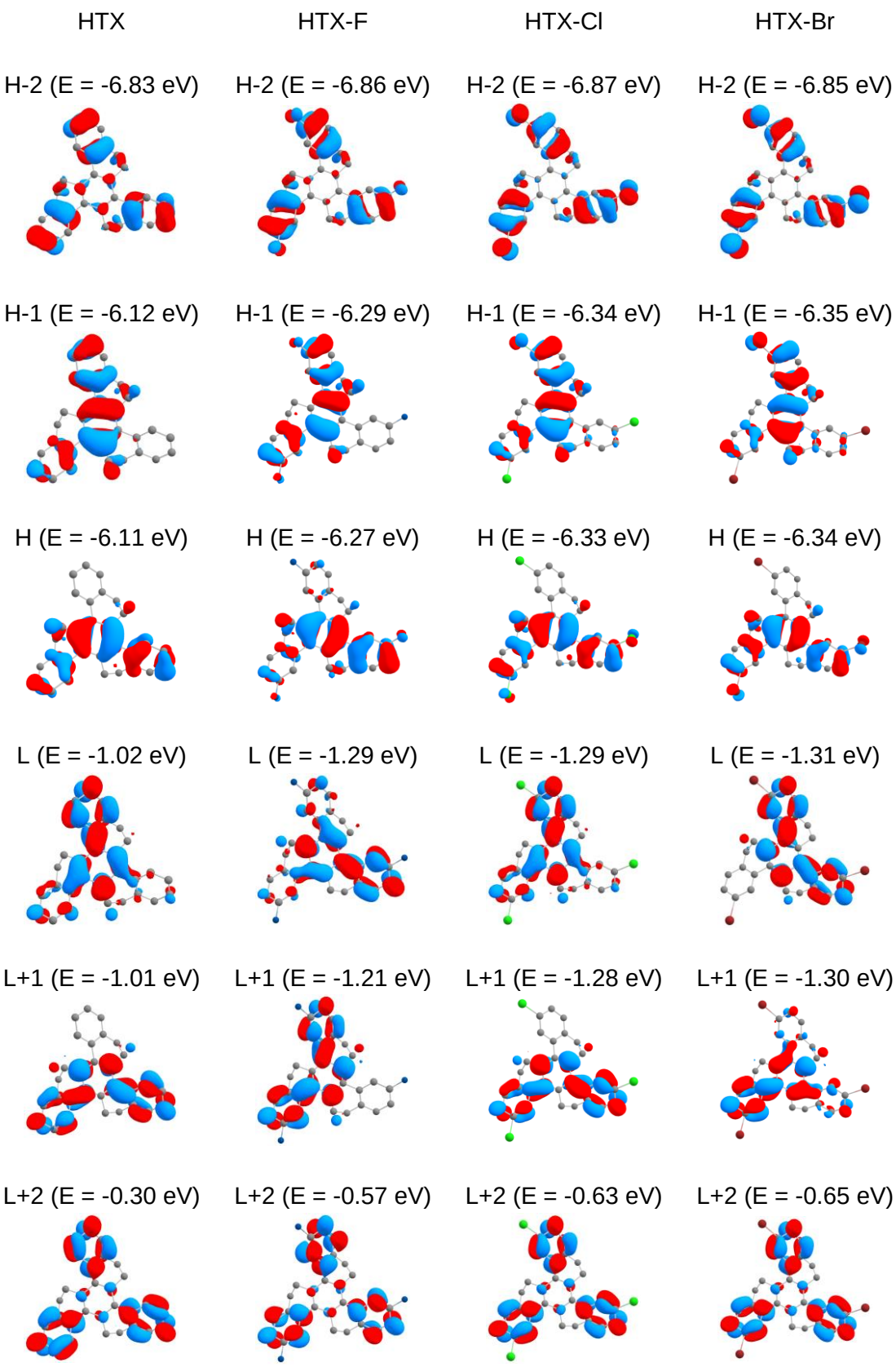

Figure S18. Frontier molecular orbitals calculated using PBE0/Def2-TZVP(-f).

Table S6. Data for the TD-DFT and SOC-TD-DFT excitations using PBE0/def2-TZVP(-f) for **HTX** in 2-MeTHF and toluene.

State	Energy		*f*	Configuration[a]
	eV	nm		
			2-MeTHF	
S_1	4.075	304	0.00017	H → L (45) H-1 → L+1 (48)
S_2	4.559	272	0.00070	H → L+1 (43) H-1 → L (47)
S_3	4.655	266	0.60124	H → L+1 (44) H-1 → L (41)
S_4	4.658	266	0.60476	H → L (41) H-1 → L+1 (44)
S_5	4.917	252	0.00640	H → L+3 (20)
T_1	3.140	395	1×10^{-9}	H → L (95)
T_2	3.531	351	2×10^{-9}	H → L+1 (39) H-1 → L (48)
T_3	3.532	351	1×10^{-9}	H-1 → L+1 (62)
T_4	3.918	316	3×10^{-9}	H-1 → L (42) H → L+1 (51)
T_5	4.038	307	23×10^{-9}	H-2 → L (27) H-1 → L+1 (16) H → L+2 (25)
T_6	4.041	307	3×10^{-9}	H-2 → L+1 (27) H-1 → L+2 (29)
			Toluene	
S_1	4.071	305	0.00017	H → L (45) H-1 → L+1 (48)
S_2	4.557	272	0.00071	H → L+1 (43) H-1 → L (47)
S_3	4.652	267	0.60387	H → L+1 (44) H-1 → L (41)
S_4	4.655	266	0.60765	H → L (41) H-1 → L+1 (44)

S_5	4.912	252	0.00631	H → L+3 (21)

[a] Transitions with high percentage contributions are shown in parenthesis.

Table S7. Data for the TD-DFT and SOC-TD-DFT excitations using PBE0/def2-TZVP(-f) for **HTX-F** in 2-MeTHF and toluene.

State	Energy		*f*	Configuration[a]
	eV	nm		
		2-MeTHF		
S_1	4.022	308	0.00166	H → L+1 (44) H-1 → L (52)
S_2	4.454	278	0.12670	H → L (82)
S_3	4.554	272	0.50306	H → L+1 (45) H-1 → L (38)
S_4	4.568	271	0.43867	H-1 → L+2 (77)
S_5	4.786	259	0.02836	H-2 → L+1 (67)
T_1	3.098	400	$>1\times10^{-9}$	H → L (90)
T_2	3.486	356	1×10^{-9}	H → L+1 (38) H-1 → L (49)
T_3	3.499	354	1×10^{-9}	H-1 → L+1 (60)
T_4	3.868	321	3×10^{-9}	H-1 → L (40) H → L+1 (50)
T_5	4.001	310	54×10^{-9}	H-2 → L (24) H-1 → L+1 (17) H → L+2 (19)
T_6	4.008	309	8×10^{-9}	H-2 → L+1 (27) H-1 → L+2 (27)
		Toluene		
S_1	4.020	308	0.00160	H → L+1 (44) H-1 → L (52)
S_2	4.452	279	0.12739	H → L (82)
S_3	4.552	272	0.50024	H → L+1 (46) H-1 → L (38)
S_4	4.564	272	0.43887	H-1 → L+2 (77)
S_5	4.765	260	0.02789	H-2 → L+1 (69)

[a] Transitions with high percentage contributions are shown in parenthesis.

Table S8. Data for the TD-DFT and SOC-TD-DFT excitations using PBE0/def2-TZVP(-f) for **HTX-Cl** in 2-MeTHF and toluene.

State	Energy		*f*	Configuration[a]
	eV	nm		
			2-MeTHF	
S_1	4.042	307	0.00037	H → L (49) H-1 → L+1 (45)
S_2	4.489	276	0.00279	H → L+1 (40) H-1 → L (48)
S_3	4.546	273	0.48022	H → L+1 (36) H-1 → L (32)
S_4	4.550	273	0.47337	H → L (32) H-1 → L+1 (37)
S_5	4.766	260	0.03286	H-2 → L (39)
T_1	3.117	398	$>1\times10^{-9}$	H → L (95)
T_2	3.490	355	$>1\times10^{-9}$	H → L+1 (38) H-1 → L (47)
T_3	3.492	355	$>1\times10^{-9}$	H-1 → L+1 (56)
T_4	3.892	319	$>1\times10^{-9}$	H-1 → L (40) H → L+1 (48)
T_5	3.960	313	4×10^{-9}	H-2 → L (20) H-1 → L+1 (17) H → L+2 (19)
T_6	3.961	313	2×10^{-9}	H-2 → L+1 (22) H-1 → L+2 (26)
			Toluene	
S_1	4.040	307	0.00038	H → L (49) H-1 → L+1 (45)
S_2	4.487	276	0.00293	H → L+1 (40) H-1 → L (49)
S_3	4.541	273	0.46906	H → L+1 (36) H-1 → L (31)
S_4	4.544	273	0.46227	H → L (32) H-1 → L+1 (36)

S_5	4.750	261	0.03412	H-2 → L (43)

[a] Transitions with high percentage contributions are shown in parenthesis.

Table S9. Data for the TD-DFT excitations using PBE0/def2-TZVP(-f) for **HTX-Br** in 2-MeTHF and toluene.

State	Energy		*f*	Configuration[a]
	eV	nm		
		2-MeTHF		
S_1	4.041	307	0.00017	H → L (28) H-1 → L+1 (27)
S_2	4.480	277	0.00931	H → L (27) H → L+1 (25) H-1 → L (25)
S_3	4.531	274	0.46003	H → L (28) H-1 → L+1 (42)
S_4	4.535	273	0.45319	H-1 → L (34) H → L+1 (38)
S_5	4.742	261	0.04457	H-2 → L+1 (38)
T_1	3.117	397	4.09×10^{-7}	H → L (89)
T_2	3.488	355	1.63×10^{-7}	H → L+1 (40) H-1 → L (44)
T_3	3.494	355	1.77×10^{-7}	H-1 → L+1 (56)
T_4	3.891	318	1.42×10^{-6}	H-1 → L (41) H → L+1 (47)
T_5	3.958	313	1.32×10^{-6}	H-2 → L (19) H-1 → L+1 (17) H → L+2 (19)
T_6	3.960	313	6.23×10^{-7}	H-2 → L+1 (21) H-1 → L+2 (26)
		Toluene		
S_1	4.039	307	0.00017	H → L (29) H-1 → L+1 (27)
S_2	4.476	277	0.00956	H → L (27) H → L+1 (25)

				H-1 → L (25)
S_3	4.524	274	0.44234	H → L (28) H-1 → L+1 (43)
S_4	4.527	274	0.43540	H-1 → L (34) H → L+1 (38)
S_5	4.720	263	0.04611	H-2 → L+1 (37)

[a] Transitions with high percentage contributions are shown in parenthesis.

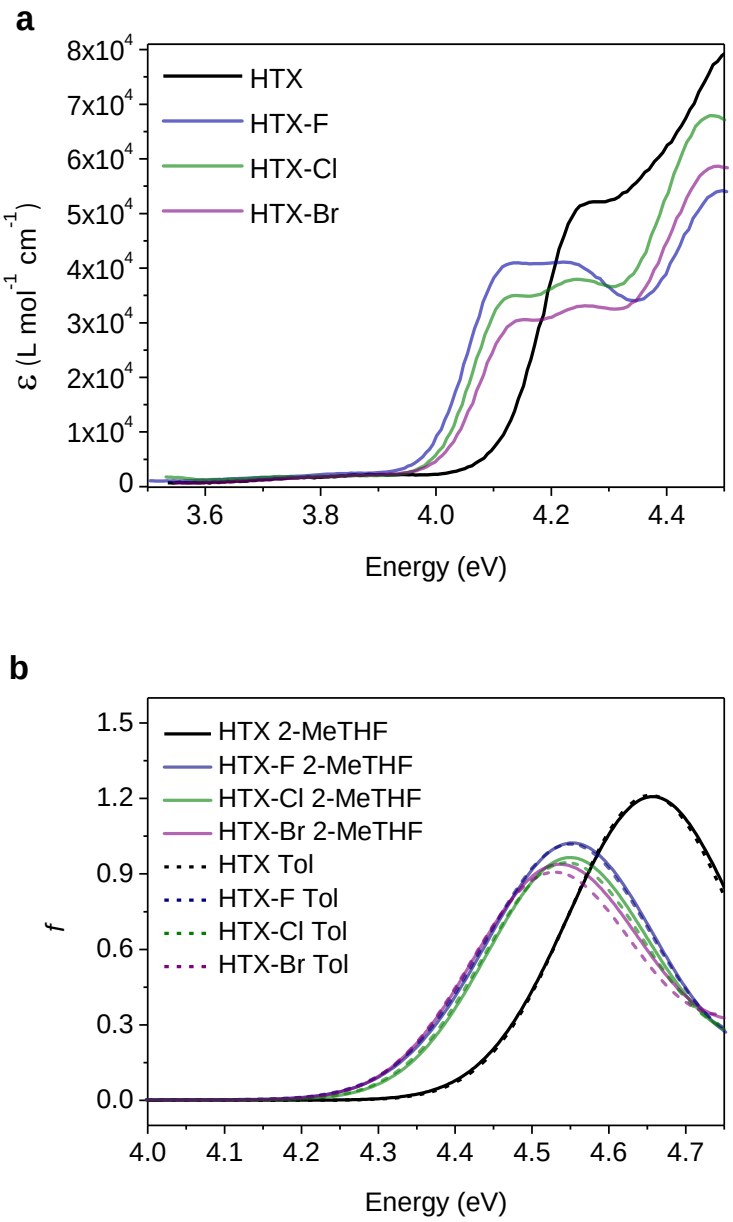

Figure S19. Experimental and theoretical spectra of **HTX** and its derivatives. (**a**) Experimental absorption spectra of **HTX** derivatives and (**b**) Theoretical absorption spectra, calculated using PBE0/ Def2-TZVP(-f) and convoluted with Gaussians of 0.25 eV width in 2-MeTHF (solid lines) and Toluene (dashed lines).

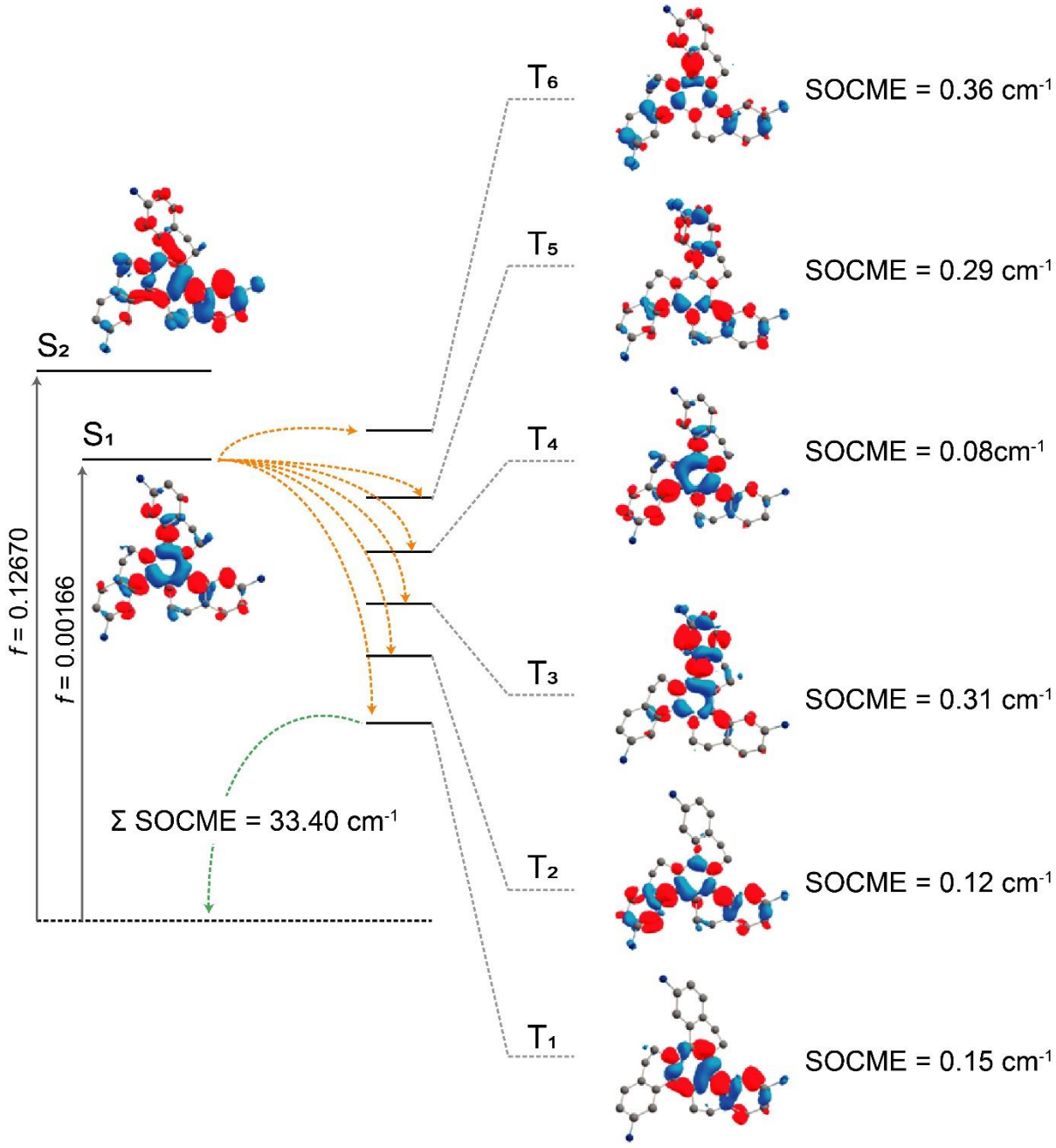

Figure S20. SOC-TD-DFT data for **HTX-F**. Modified Jablonski diagram for **HTX-F** and calculated SOCME for $S_1 \rightarrow T_n$ transition (orange arrows) at the S_1 optimized geometry and for the $T_n \rightarrow S_0$ transition (green arrow) at the T_1 optimized geometry. The SOCME was calculated using $\sqrt{\Sigma\langle T_{j\,(MS=0,\pm1)}|\, H_{SO}\, |S_i\rangle^2}$ and the ΣSOCME is the sum of all matrix elements between the first ten singlet and triplet states, $\Sigma\langle T_{1\text{-}10}|H_{SO}|S_{0\text{-}10}\rangle$. The OS for S_1 and S_2 is shown as vertical arrows.

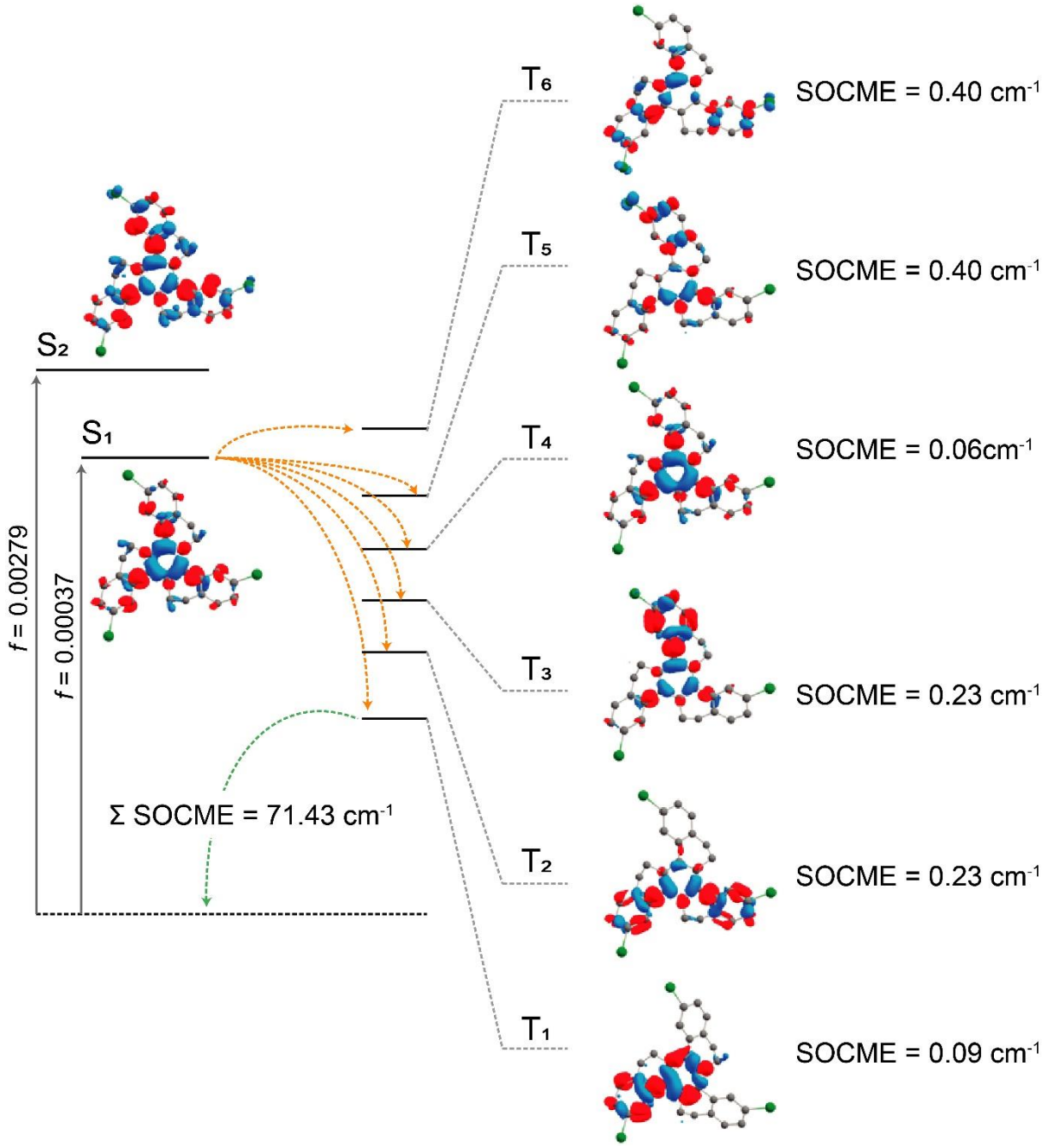

Figure S21. SOC-TD-DFT data for **HTX-Cl**. Modified Jablonski diagram for **HTX-Cl** and calculated SOCME for $S_1 \rightarrow T_n$ transition (orange arrows) at the S_1 optimized geometry and for the $T_n \rightarrow S_0$ transition (green arrow) at the T_1 optimized geometry. The SOCME was calculated using $\sqrt{\Sigma\langle T_{j\,(MS=0,\pm1)}|\, H_{SO}\, |S_i\rangle^2}$ and the ΣSOCME is the sum of all matrix elements between the first ten singlet and triplet states, $\Sigma\langle T_{1\text{-}10}|H_{SO}|S_{0\text{-}10}\rangle$. The OS for S_1 and S_2 is shown as vertical arrows.

Table S10. SOC, adiabatic energy difference, Root-mean-square deviation (RMSD) of atomic positions using S_0 as reference and decay rates for **HTX** and its homologs.

		HTX	**HTX-F**	**HTX-Cl**	**HTX-Br**
SOCME	$\Sigma\langle T_{1\text{-}10}\|H_{SO}\|S_{0\text{-}10}\rangle$ [a] (cm^{-1})	33.48	34.21	72.24	451.73
	$\Sigma\,\Sigma\,\langle T_{1\text{-}6}\|H_{SO}\|S_1\rangle$ [b] (cm^{-1})	1.13	1.32	1.41	4.53
Energy of the states	S_1 [c] (eV)	3.44	3.39	3.39	3.39
	S_2 [c] (eV)	3.74	3.57	3.47	3.62
	S_3 [c] (eV)	3.97	3.62	3.66	3.82
	T_1 [c] (eV)	2.74	2.71	2.73	2.78
RMSD	S_1 [d]	0.0858	0.1918	0.1052	0.0988
	S_2 [d]	0.2982	0.0990	0.1823	0.1682
	T_1 [d]	0.2540	0.1103	0.1808	0.6069
S_1 decay rates	k_r (Theo) $\times 10^7$ (s^{-1}) [e]	0.55 (99)	1.31 (89)	1.24 (97)	1.36 (99)
S_2 decay rates	k_r (Theo) $\times 10^9$ (s^{-1}) [e]	1.90 (100)	1.81 (93)	4.52 (100)	5.89 (99)
T_1 decay rates	k_r (Theo) (s^{-1}) [e]	32.61 (100)	6.67 (100)	8.11 (100)	91.90 (100)

[a] $\sqrt{\Sigma\langle T_{j\ (MS=0,\pm1)}|\ H_{SO}\ |S_i\rangle^2}$ at the T_1 optimized geometry; [b] $\sqrt{\Sigma\langle T_{j\ (MS=0,\pm1)}|\ H_{SO}\ |S_i\rangle^2}$ at the S_1 optimized geometry; [c] Adiabatic energy; [d] Comparted to the ground state geometry. [e] Values in parentheses are the percentage of HT.

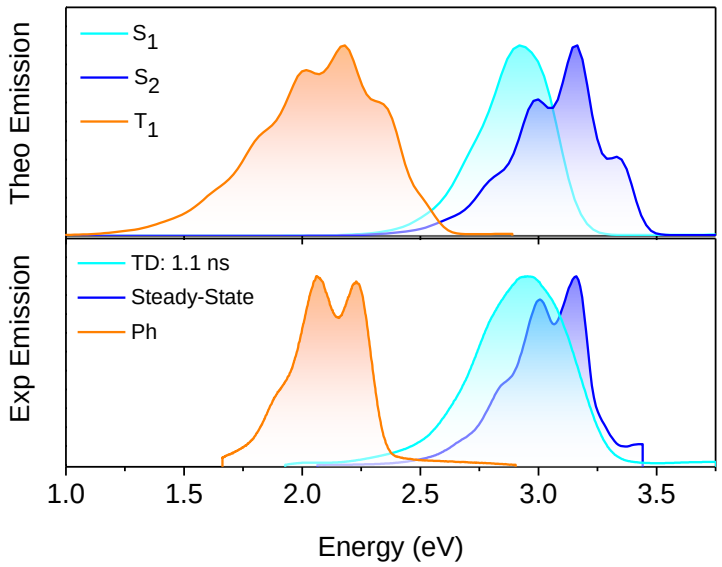

Figure S22. Experimental and predicted normalized fluorescence and phosphorescence using PBE0/ Def2-TZVP(-f) and the path-integral approach for **HTX-F**. The singlet 0–0 energy difference was red-shifted by 0.30 eV for S_1 and by 0.20 for S_2 emission to match the experimental data.

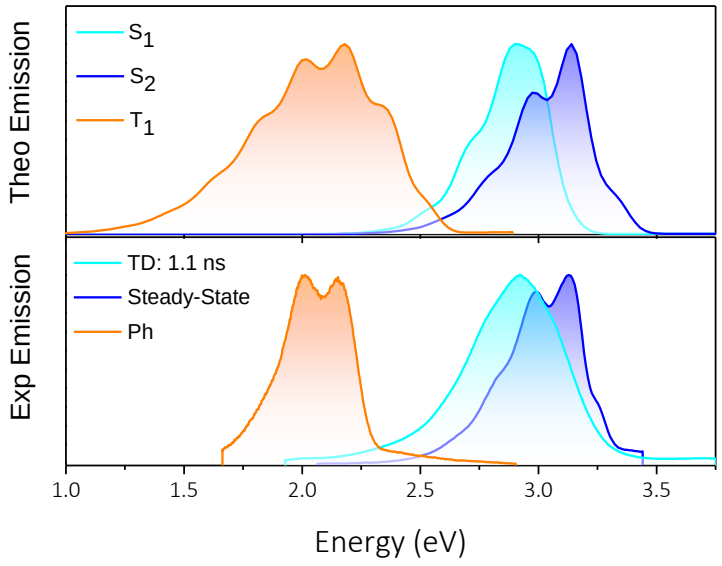

Figure S23. Experimental and predicted normalized fluorescence and phosphorescence using PBE0/Def2-TZVP(-f) and the path-integral approach for **HTX-Cl**. The singlet 0–0 energy difference was red-shifted by 0.30 eV for S_1 and by 0.10 for S_2 emission to match the experimental data.

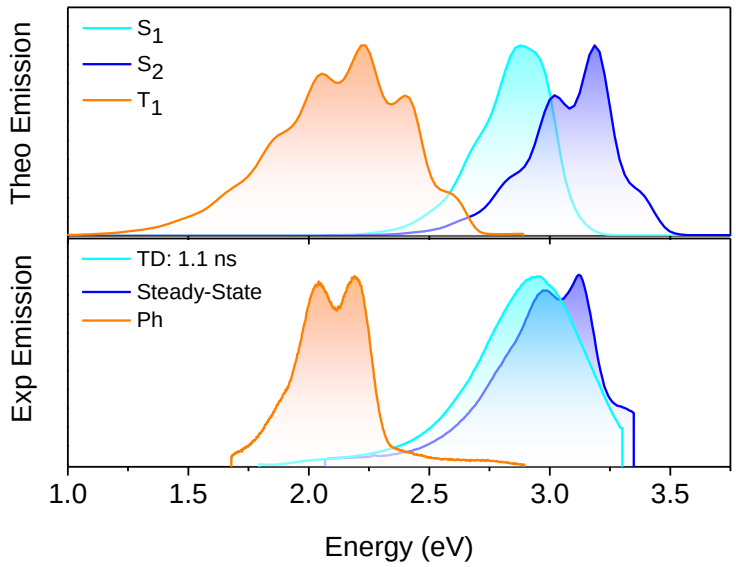

Figure S24. Experimental and predicted normalized fluorescence and phosphorescence spectra using PBE0/ Def2-TZVP(-f) and the path-integral approach for **HTX-Br**. The singlet 0–0 energy difference was red-shifted by 0.30 eV for S_1 and by 0.20 for S_2 emission to match the experimental data.

^{1}H, ^{13}C and ^{19}F NMR Data

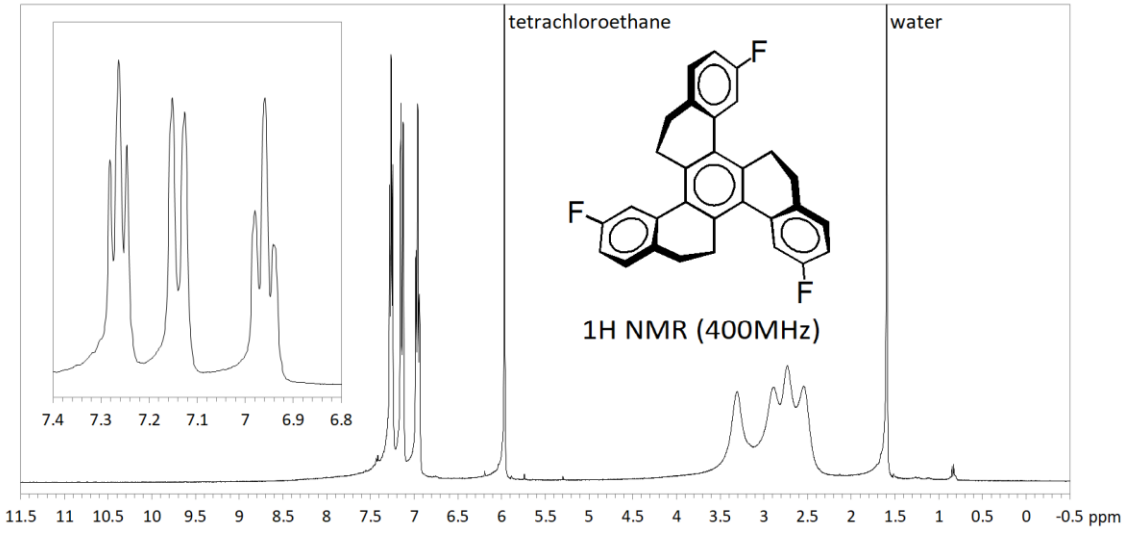

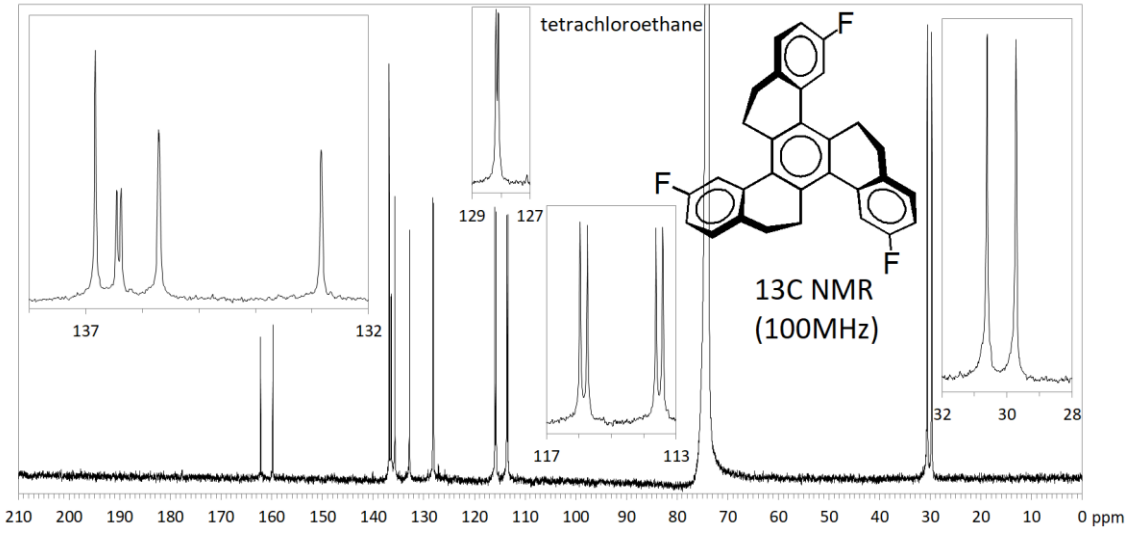
tetrachloroethane
F
F
F
13C NMR
(100MHz)
137
132
129
127
117
113
32
30
28
210 200 190 180 170 160 150 140 130 120 110 100 90 80 70 60 50 40 30 20 10 0 ppm

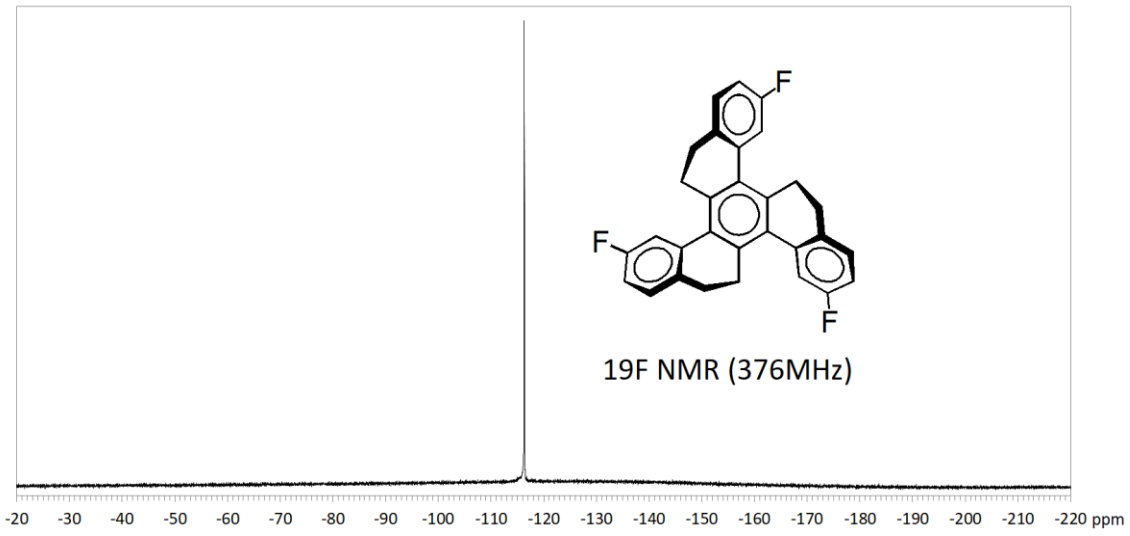
F
F
F
19F NMR (376MHz)
-20 -30 -40 -50 -60 -70 -80 -90 -100 -110 -120 -130 -140 -150 -160 -170 -180 -190 -200 -210 -220 ppm

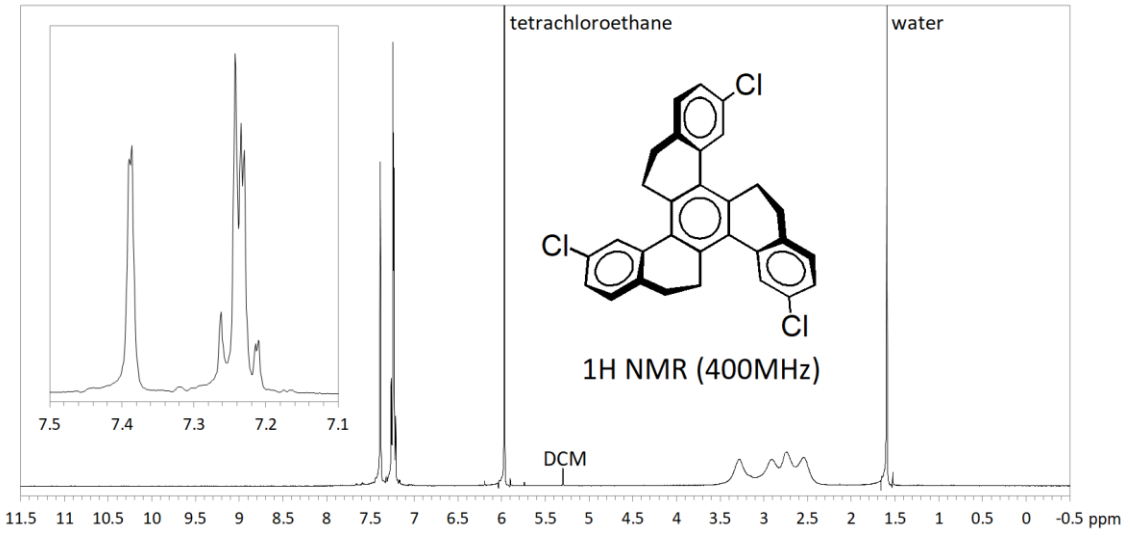
tetrachloroethane
water
Cl
Cl
Cl
1H NMR (400MHz)
DCM
7.5
7.4
7.3
7.2
7.1
11.5 11 10.5 10 9.5 9 8.5 8 7.5 7 6.5 6 5.5 5 4.5 4 3.5 3 2.5 2 1.5 1 0.5 0 -0.5 ppm

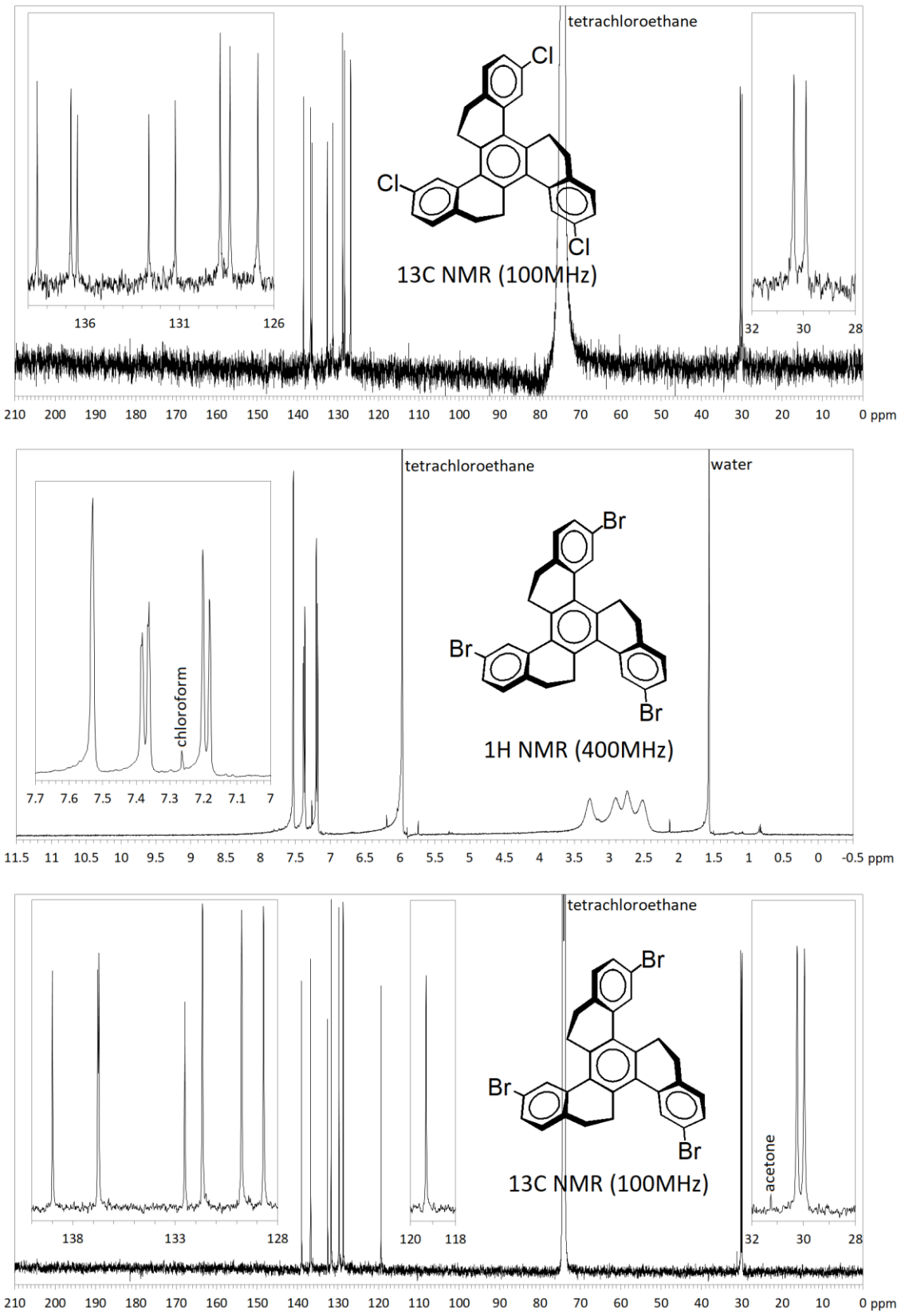

Figure S25. ^{1}H, ^{13}C and ^{19}F NMR spectra.